UMS
UNIVERSITI MALAYSIA SABAH

BORNEO SCIENCE

The Journal of Science and Technology

ONLINE ISSN : 2231-9085 | ISSN : 1394- 4339

BORNEO SCIENCE

A JOURNAL OF SCIENCE AND TECHNOLOGY

BORNEO SCIENCE is a journal of science and technology published twice a year. It publishes original articles on all aspects of research in science and technology of general or regional interest particularly related to Borneo. Manuscripts submitted must not have been published, accepted for publication, or be under consideration elsewhere. Borneo Science welcomes all categories of papers: full research papers, short communications, papers describing novel methods, review papers and book reviews. Views expressed in the articles do not represent those of the Editorial Board and the University.

BORNEO *SCIENCE* *merupakan jurnal sains dan teknologi yang diterbitkan dwitahunan. Jurnal ini menerbitkan artikel asli dalam kesemua bidang sains dan teknologi secara umum mahupun dalam kepentingan serantau, terutamanya yang berkaitan dengan Borneo. Manuskrip yang dihantar bukan yang telah diterbitkan, telah diterima untuk diterbitkan, atau sedang dipertimbangkan untuk diterbitkan. Borneo Science mengalu-alukan semua jenis kertas kerja sama ada hasil penyelidikan, komunikasi pendek, penjelasan suatu kaedah, ulasan kertas kerja atau ulasan buku. Pandangan yang ditulis dalam artikel Borneo Science tidak menggambarkan pendapat Sidang Editor dan Universiti.*

DOI: https://doi.org/10.51200/bsj.v44i1

BORNEO SCIENCE
A JOURNAL OF SCIENCE AND TECHNOLOGY

BORNEO SCIENCE

A JOURNAL OF SCIENCE AND TECHNOLOGY

ONLINE ISSN 2231-9085 | ISSN 1394-4339

BORNEO SCIENCE

A JOURNAL OF SCIENCE AND TECHNOLOGY
JURNAL SAINS DAN TELNOLOGI

Volume 44 Issue 1

March 2023

CONTENT
KANDUNGAN

Page
Muka
Surat

ORIGINAL ARTICLES

BorneoScience
The Journal of Science & Technology
Volume 44 Issue 1 : April 2023
Online ISSN : 2231-9085 | ISSN : 1394-4339

WEATHER EVENTS FORECASTING IN KOTA KINABALU USING A FUZZY RULE-BASED SYSTEM

Suzelawati Zenian and Amirah Ramizah Bibi Abdul Rasheed

Mathematics with Computer Graphics, Faculty of Science and Natural Resources, Universiti Malaysia Sabah, Jalan UMS, 88400 Kota Kinabalu, Sabah, Malaysia.

Corresponding author. Email: suzela@ums.edu.my

Received 13th November 2021; accepted 12th March 2022
Available online 20th April 2023
Doi: https://doi.org/10.51200/bsj.v44i1.4336

ABSTRACT. *A weather forecast is a prediction of weather phenomena in the future by collecting as much data as possible. Major worldwide climate studies include the breakthrough and interpretation of complicated weather patterns in order to successfully forecast varied weather events. It is quite complex to screen so many parameters from several factors to discover precise weather conditions. In this paper, a fuzzy rule-based system (FRBS) is applied for weather forecasting in Kota Kinabalu. There are 234 fuzzy rules being developed as the FRBS are constructed along and successfully implemented in MATLAB. Based on the results, the comparison between actual and forecast data shows moderate precision as the accuracy level is higher than the level of error analysis.*

KEYWORDS. Weather events, fuzzy rule-based system, forecasting, fuzzy set.

INTRODUCTION

Malaysia is an Asian country situated north of the equator and is geographically located in between two large oceans which are the Pacific Ocean to the east and the Indian Ocean to the west (Malaysia Meteorological Department, 2016). There is no dry season in Malaysia because it is near the equator, which is also surrounded by oceans. In general, as is the case in tropical countries, Malaysia experiences a rainy season which is relatively unpredictable every year. The study area is Kota Kinabalu, Sabah, one of Malaysia's states. The selected location for this study will be southwest of Kota Kinabalu city. The existing weather forecasting research is performed within the same area using a soft computing technique (Mojiol, 2006). There are data sets from January 2019 to December 2019 on probability distribution for the development of weather forecasts. This region has a typical moist continental climate. The conditions are regularly hot and cool, with strong rainfall typically in the afternoon and highly unchanging all year long.

Weather forecast is a significant issue that must be considered because of the variability of human activities which will eventually regulate the weather in a region of a country. All human activities such as the variations in land refuge and the burning of fossil fuels, are alleged to be one of those contributions to this issue of constant changes in the weather. Fuzzy logic stipulates an effective technique to relate to the weather parameter and the weather events. To complete the research, a software called MATLAB will be used to implement the generated FRBS by using certain MATLAB

functions (Moler & Little, 2020). Khatua *et al.* (2020) showed that in order to investigate the impact of global warming, water pollution, and harvesting of juvenile fishes on the production of mature Hilsa fishes, a mathematical model is developed using fuzzy inferences. Cihan (2020) implemented FRBS to forecast the number of verified cases in the Covid-19 outbreak in Turkey.

Fuzzy logic is also used to forecast relative humidity because fuzzy logic can manage weather uncertainty and complexities despite dealing with major mathematical terms. Fuzzy logic is a simple but effective technique for solving problems with comprehensive applications. Fuzzy logic can be used to provide alternatives for unclear, inaccurate, and ambiguous issues. Fuzzy logic is another of those logical or expert systems, the purpose where it is to use the expertise and experience acquired over a period to achieve a human expert level (Ross, 2010; Zadeh, 1975).

This paper focuses on the implementation of FRBS in forecasting the weather events in Kota Kinabalu based on the data collection from the Meteorology Forecasting Department in Kota Kinabalu. In this paper, the observation of daily weather events will include temperature, relative humidity, atmospheric pressure, and precipitation. Then these weather observations will be used as parameters related to forecast the selected weather events such as rain, thunderstorm, rain-thunderstorm, cloudy and sunny.

Hence, a mapping of the weather parameters onto weather events has to be developed in order to be able to predict the weather event. This can be done by implementing FRBS in the MATLAB software by undergoing a few processes such as fuzzification, rule generation, rule-based reduction and inferencing. Then the forecasted weather events will be compared with the actual data to clarify the differences in order to determine the precision of accuracy and error analysis. As a result, forecasting the weather event can be accomplished because the fuzzy logic stipulates an effective technique to relate to weather parameters and weather events as it is fuzzy in nature. Thus, this can contribute more to the meteorology field.

MATERIALS AND METHODS

To develop the FRBS in forecasting weather events, there are a few processes in developing the fuzzy rules shown in the experimental setups (Sharma *et al*., 2014). There are eight steps to be implemented whereby the performances will be compared according to the monthly forecast data which will then determine the accuracy and error analysis. The measures engaged are summarized in the remaining discussion for this section.

The process segment can be extended in detail as the steps in conducting these processes are dependent on each other. Firstly, it is the development of FRBS by applying the data set. Secondly, the results of monthly data of the original weather events and the forecasted weather events would be measured in a plot to display the inconsistency between them and evaluate the precision for accuracy analysis and error analysis. Ultimately, a summary will be included in the last stage which is the conclusion to summarize the important elements. There are eight steps opted in developing the fuzzy rules in this experimental setup as illustrated in Figure 1

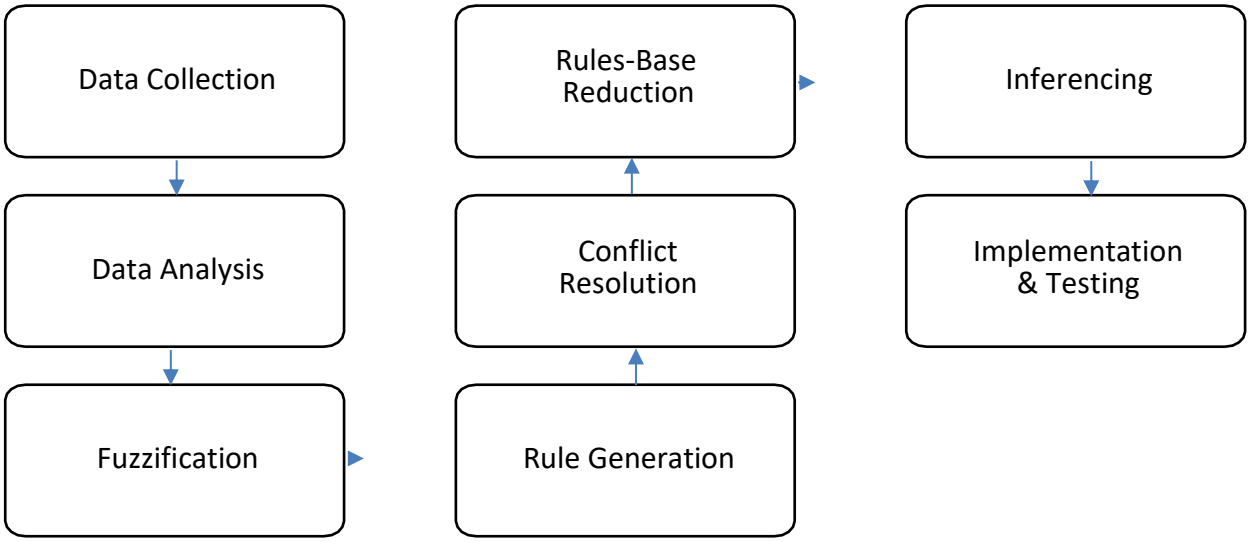

Figure 1. Methodology for developing the FRBS

A. *Data Collection*

Daily weather observations from January 2019 to December 2019, a total of one year of weather parameters such as temperature, humidity, precipitations and atmospheric pressure. The data collected are from the Malaysia Meteorology Department (2016).

B. *Data Analysis*

Data are collected to determine if the extreme data exist, the errors collection and the sample size of data included in this weather forecasting can be recognized. Due to the common occurring weather events in Malaysia, there are five forms of weather events preferred in forecasting the weather which are the "Rain", "Rain-Thunderstorm", "Thunderstorm", "Cloudy" and "Sunny" weather events. There are four types of weather observation which are atmospheric pressure, precipitation, humidity, and temperature which have been gathered for data analysis.

C. *Fuzzification of input/output*

The fuzzification will assign a range of linguistic variables that define the various input and output parameters of the system. Fuzzification is the step by which the crisp values are fuzzified into membership levels associated with the fuzzy sets. A triangular shape membership function has been selected as the input variable ranges from 0 to 1 in a specified discourse universe. The linguistic variables which are applied are "very low", "low", "medium", "high" and "very high" along with the four-input variable which are atmospheric pressure, precipitation, humidity, and temperature. The range for the weather parameters is defined by determining the maximum and minimum numerical value of each weather parameter.

D. *Rule Generation*

Through engaging MATLAB rules editor, the rules are incorporated into the fuzzy inference system. The automatic generating of rules is utilized to generate the automatic specific rules by applying an algorithm based on the collected weather data to produce the data extraction. Apart from that, the engagement with human specialists relying on their perspectives, heuristic based and preferences resulting in a standardized rule set.

E. Conflict Resolution

The indicator of conflict resolution is a decoding process of outputs called defuzzification whereby the multiple fuzzy rules were compared and cancelled. The conflict resolution is accomplished by carrying out in the fuzzy rule-based system by initial classification of the generic and specific rules that are created followed by removing the inconsistent and redundant rules before ultimately aggregation of rules is performed.

F. Inferencing

The Mamdani inference framework is used in the forecasting system. The application of Mamdani inference framework is required to develop the dynamic fuzzy sets as the output product membership functions. Following the aggregation method, for every output variable, a fuzzy set exists which needs to undergo defuzzification process. A list of sample fuzzy rules is shown in Table 1.

Table 1. Developed fuzzy rules.

Rules	IF (antecedent)	THEN (consequence)
1	(TodayTemp is low) and (YestTemp is high) and (TodayPressure is low) and (YestPressure is medium)	forecast is cloudy
2	(TodayTemp is high) and (YestTemp is high) and (TodayPressure is medium) and (YestPressure is medium)	forecast is clear
3	(TodayTemp is high) and (YestTemp is high) and (TodayHumidity is low) and (YestHumidity is low)	forecast is sunny
4	(TodayTemp is high) and (YestTemp is high) and (TodayPressure is medium) and (YestPressure is low)	forecast is thunder
5	(TodayTemp is low) and (YestTemp is medium) and (TodayHumidity is VHigh) and (YestHumidity is VHigh)	forecast is rain
6	(TodayTemp is high) and (YestTemp is high) and (TodayPressure is VLow) and (YestPressure is low)	forecast is rain-thunder

G. Implementation & Testing

To show the output of the outcome for forecasting weather events, this system will be implemented in MATLAB R2018 software which is the key factor for this weather forecast. The rules editor in MATLAB is used to apply specific and generic rules. The implementation of FIS is described as the shaping of the consequence part (Then) based on the antecedent part (If) and the inputs are fuzzy subsets. To conclude briefly regarding the fuzzy RBS in the experimental setup, it will have the following basic characteristics for this methodology as shown in Table 2.

Table 2. Basic characteristics

Linguistic Labels (Input)	4
Number of outputs	8
Number of rules	234
Inferencing Method	Forward Chain
Inference model	Mamdani
Aggregation Operator	"MIN"

H. Determine Precision

The experimental setup findings above could be used to improve weather prediction accuracy based on the statistics obtained. Generally, experiments require a precision analysis or error analysis in order to correlate the usual outcome and evaluate the accuracy and the error analysis in percentage. The formulae applied throughout this paper to determine the precision by calculating the error analysis and the predictive accuracy analysis are shown as follows (Sharma *et al.*, 2014).

$$\text{Relative Error} = \frac{\text{Absolute Error}}{\text{Actual Value}} = \frac{\text{Actual Value - Observed Value}}{\text{Actual Value}} \quad (1)$$

$$\text{Error Analysis} = \text{Percentage relative error} = \text{Relative error} \times 100\% \quad (2)$$

$$\text{Accuracy analysis} = \text{Percentage accuracy} = 100\% - \text{Error analysis} \quad (3)$$

DESIGN AND IMPLEMENTATION

This section outlines the fuzzy logic toolbox as the system implementation which are effective in helping user step-by- step in developing a system design of fuzzy inference system. Fuzzy Logic Toolbox comprises several MATLAB features, tools, and a Simulink framework for analyzing, constructing, and modelling systems based on fuzzy logic. In fuzzy logic toolbox there are five main components which consist of Fuzzy Logic Designer, Surface Viewer, Rule Editor, Membership Function Editor and Rule Viewer which will be explained in further details. There are directions, stages and usage for each of the boxes which are relevant to the information of a system to be designed (Agboola, 2013, Awan & Awais, 2011, Hemayatkar, 2018).

A. Input

The input is the weather event data.

B. Process

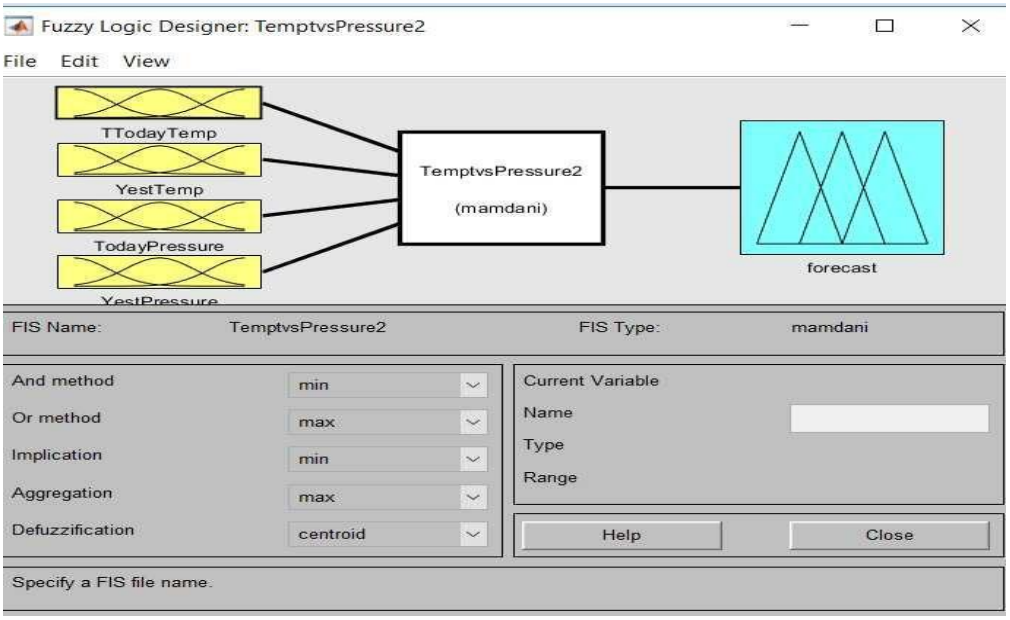

Figure 2. Fuzzy Logic Designer

User can build and evaluate fuzzy inference system for modelling a complex system behavior with the aid of fuzzy logic designer application (see Figure 2). There is no limited number of data entry in the fuzzy logic designer. If the data entry and membership function are high, it will be a problem in interpreting the outcomes for an inference system. Moreover, user can modify and build an appropriate model inference system using this fuzzy logic designer display box.

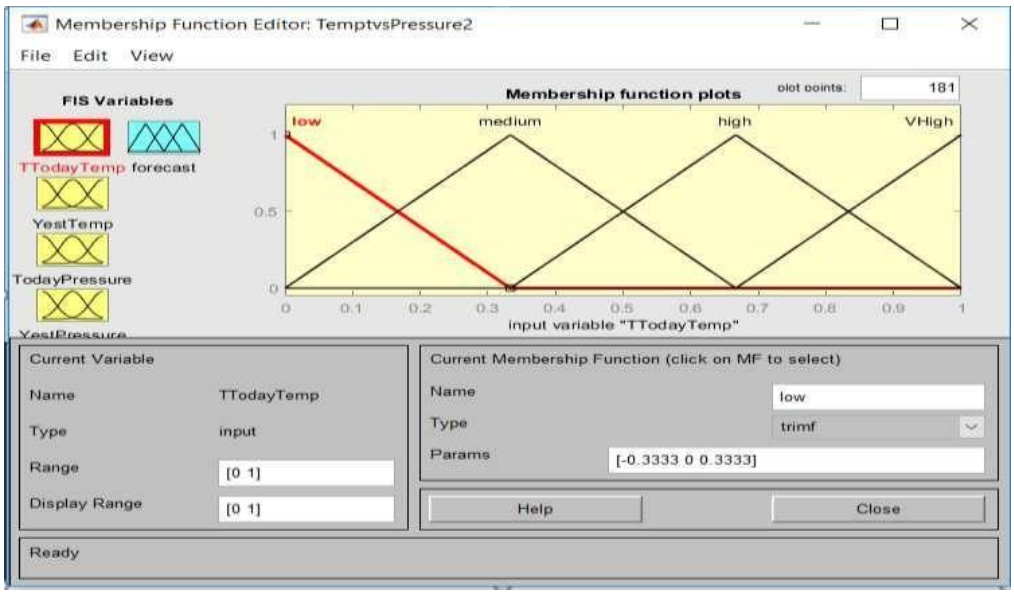

Figure 3. Membership Function Editor

The membership function editor is a method for viewing and modifying all membership features associated and enables a user to manipulate input and output data for entire fuzzy inference system. Users can also view the membership function plots which are shown in Figure 3 above for the variable which are selected.

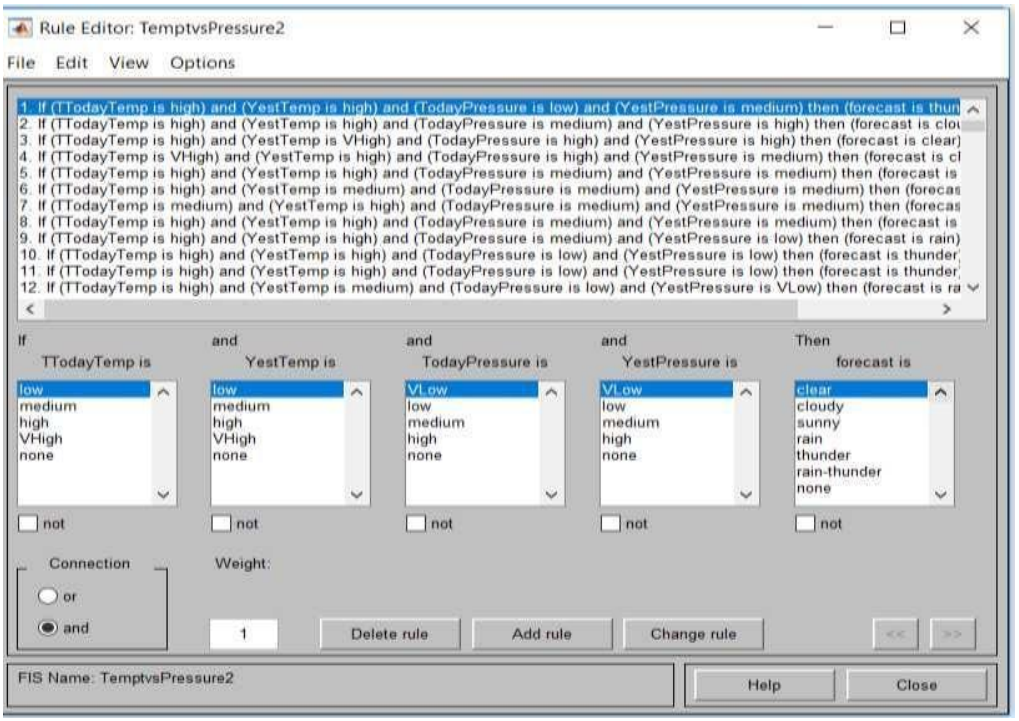

Figure 4. Rule Editor

The rule editor box is widely used to create an IF-THEN network. This is because the rule editor allows the user to build the rule statements. A collection of rules can be generated automatically depending on the input variable which is set in the box as shown in Figure 4.

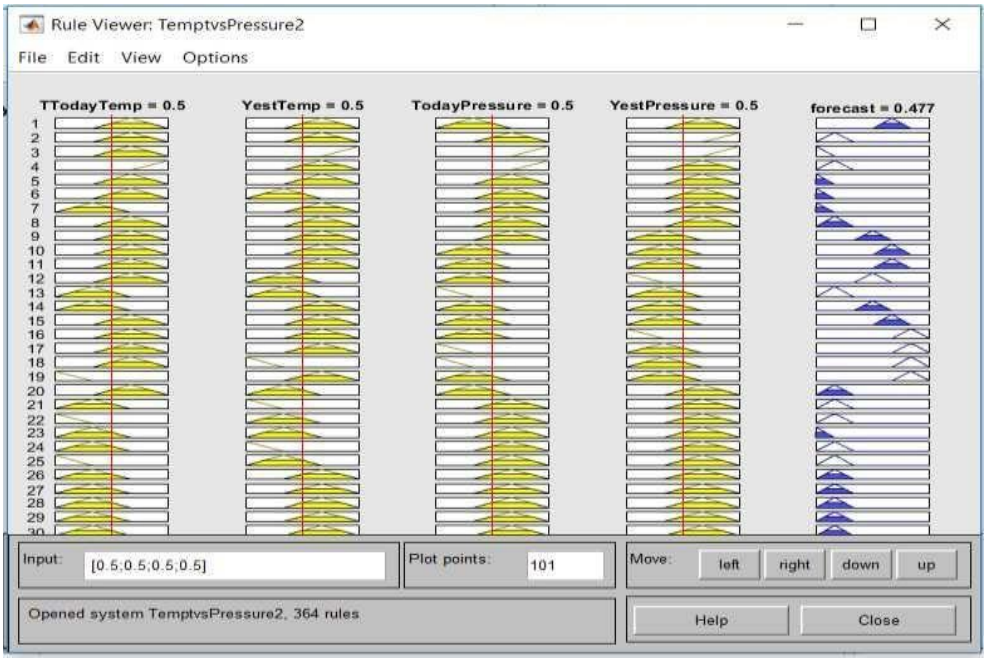

Figure 5. Rule Viewer

The overall results of the fuzzy inference process will be shown in the rule viewer section. Users can observe a new screen of a diagram pop-up with numerous graph plots embedded within it. The rule viewer will illustrate and shows a set of membership function in every column (see Figure 5).

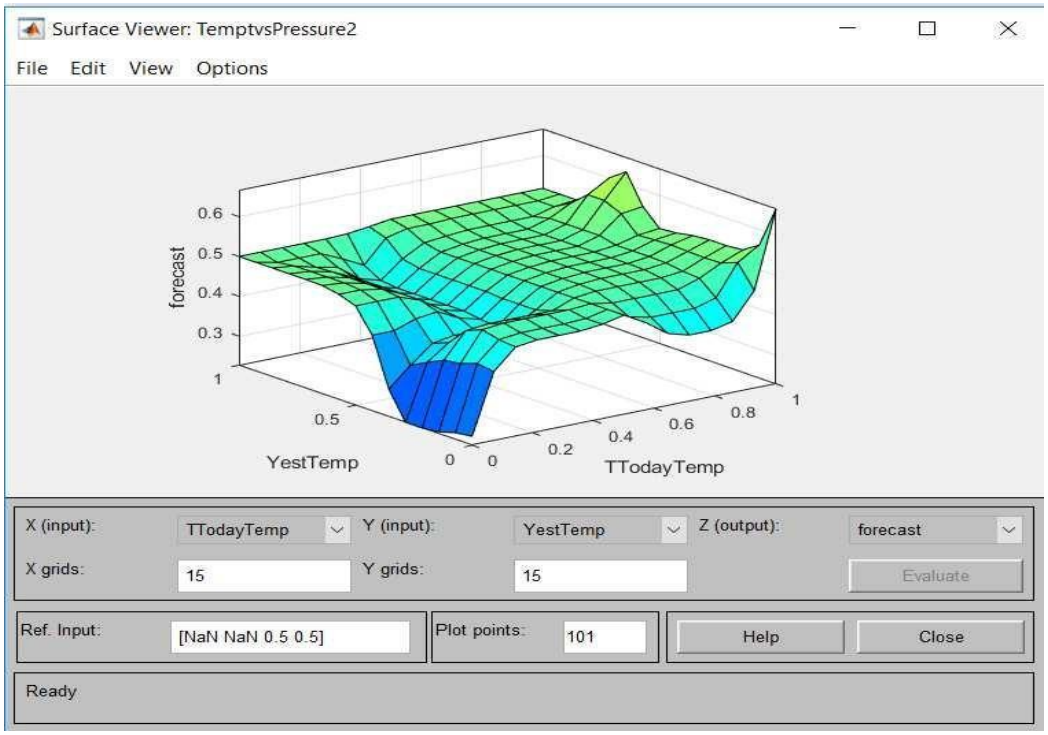

Figure 6. Surface Viewer

In the surface viewer (see Figure 6), it will display the surface that represents the mapping of the membership function where the three-dimensional of *x* is for input, *y* is for input and *z* is for the output.

C. Output

The output will be used as parameters related to forecasting the selected weather events such as rain, thunderstorm, rain-thunderstorm, partly cloudy and sunny. Hence, the mapping of weather parameters onto weather events must be developed to obtain the forecasted weather events. In this study, a comparison of the forecast events will be made to display the wider view of forecasting data of the fuzzy rules and the data accuracy will be calculated to increase the accuracy of forecasting data of the fuzzy rules.

RESULTS AND DISCUSSION

The results are conducted by implementing MATLAB software and will be discussed in detail. Besides, the accuracy of the forecasting will be examined. There are 234 sets of rules which are successfully developed by focusing on the data and the weather event in the year 2019. The successfully developed rules consist of 29 rules for cloudy weather events, 42 rules for sunny weather events, 20 rules for thunderstorm weather events, 63 rules for rain weather events, and 80 rules for rain- thunderstorm weather events.

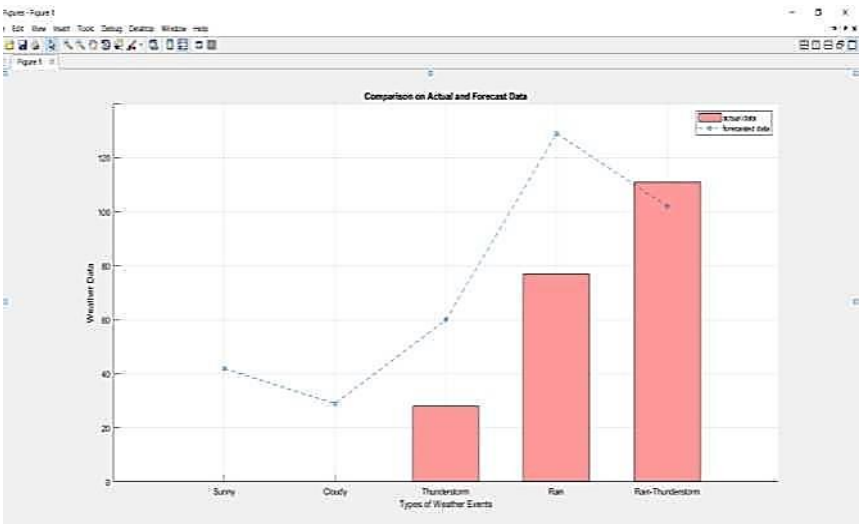

Figure 7. Comparison of actual and forecasted data

Figure 7 portrays the comparison in total number of forecasted data which have moderate precision of accuracy with the actual weather events in days using graph plotting. The actual data are represented using the bar chart graph whereas the forecast data are represented by the line graph plotting. It is clearly illustrated that the forecast data exceeded the actual data value for "Thunderstorm" and "Rain" weather events. Moreover, there are no actual data for "Sunny" and "Cloudy" weather events, so the data could not be compared with the forecast data. Thus, the plotting indicates that the forecast data is higher in majority weather event as compared to actual data which contain some missing value.

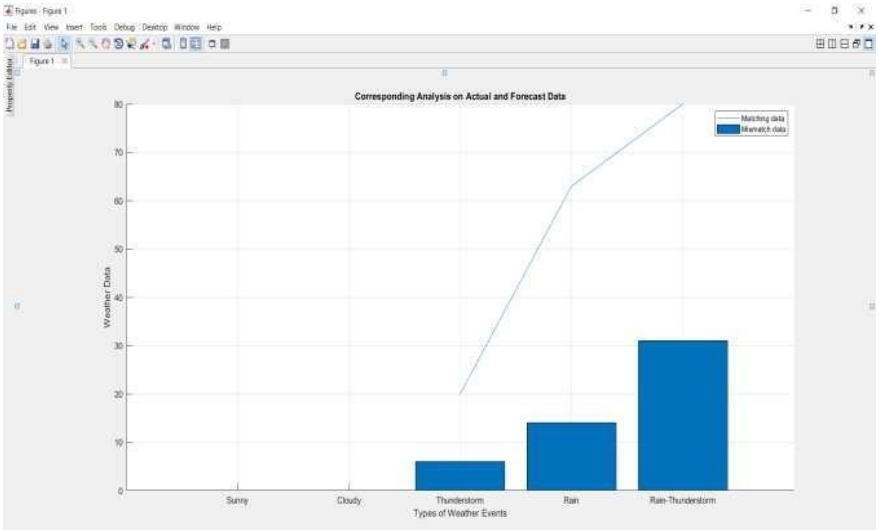

Figure 8. Corresponding analysis of match and mismatched data

Figure 8 portrays the corresponding data between matching and mismatched data for the actual and forecast weather event. This clearly illustrated that the matching data are higher than the mismatch data in total for the year 2019. The highest matching data are for "Rain- Thunderstorm" weather event with 80 matching data corresponding to actual and forecast weather events. Apart from that, for "Rain" weather event, there are 63 matching data which marked the second highest matching data whereas as much as 20 matching data for "Thunderstorm" weather event corresponds to actual and forecast weather events.

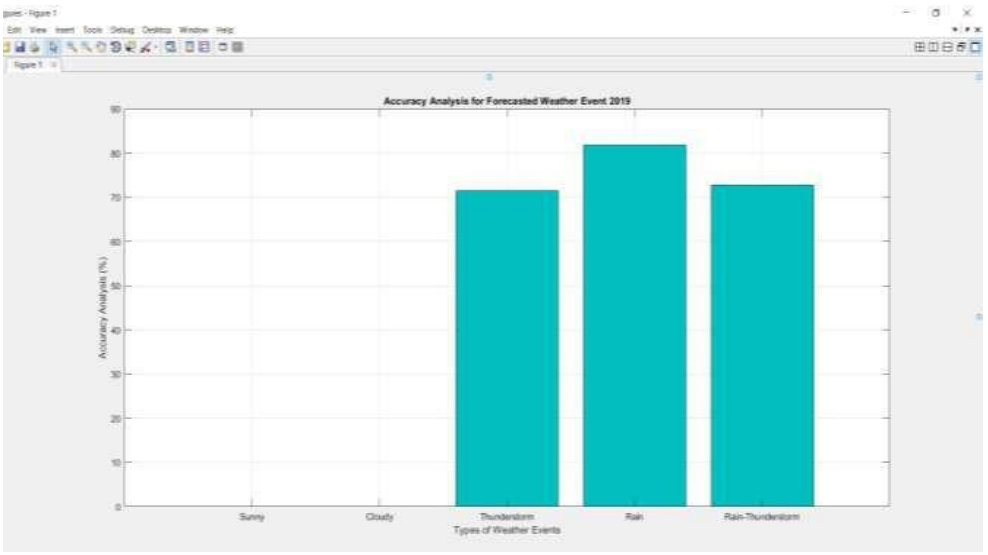

Figure 9. Accuracy analysis for forecasted weather event

Figure 9 portrays the precision of accuracy for forecasted weather events in percentage using bar graph plotting. The overall precision of accuracy is obtained by 75.5% for all three weather events. There are three weather events data been plotted which are “Rain”, “Thunderstorm” and “Rain-Thunderstorm”. Among the three, only “Rain” weather event managed to achieve the highest precision of accuracy compared to the other two weather events.

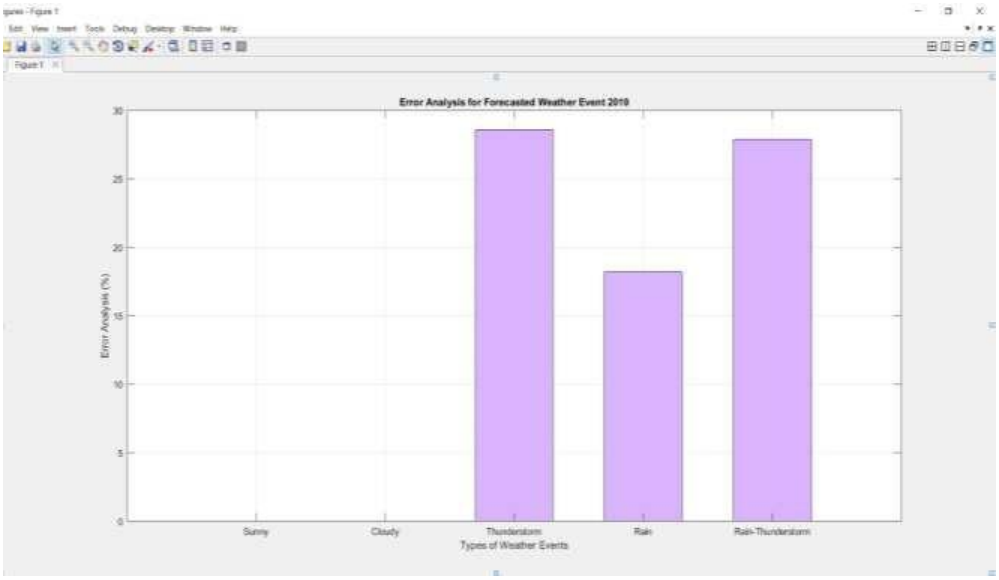

Figure 10. Error analysis for forecasted weather event

Figure 10 illustrates the error analysis for the three weather events resulting in a total error analysis of 23.6%. Among the weather events there are two weather events with high error analysis which are ‘Rain-Thunderstorm” and “Thunderstorm”. Nevertheless, compared to the three-weather event, the lowest error analysis is the “Rain” weather event resulting in 18.2%. However, there is no outcome for the "Sunny" and "Cloudy" weather events because there is no actual data available.

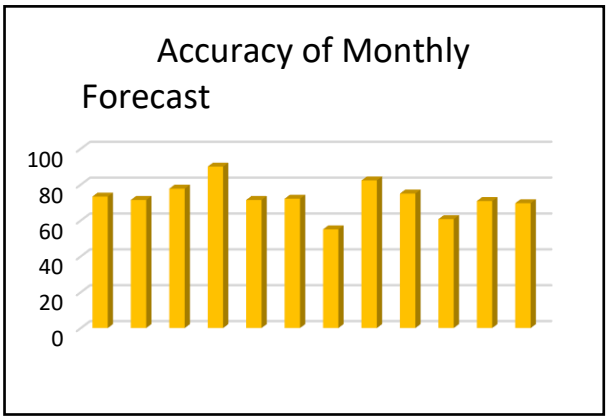

Figure 11. Monthly forecast of accuracy analysis

To sum up, an overall plotting of graph has been performed to show the differences in terms of months for the precision of accuracy for the forecasting weather events. The month which has the highest precision of accuracy is in April with approximately 90% accuracy and followed by March, August and September with approximately 70% to 80% accuracy. However, there were two months which marked the lowest precision of accuracy. They are the month of July and October with approximately 55% and 65% respectively. The obvious low accuracy of the forecast weather is due to scarcity of a rule that could be developed including the existence of several missing events that could contribute to low accuracy.

CONCLUSION

This paper has discussed in detail regarding the method of a fuzzy rule-based system in developing the rules for forecasting weather events. The implementation of FRBS have been positively accomplished by utilizing the software which is MATLAB R2018a. In particular, this paper is executed for several reasons in order to track and determine the weather event in Kota Kinabalu, Sabah. It is quite a beneficial and effective method to achieve the objective of this experiment. Another success is when 178 fuzzy rules were developed based on the actual weather data by using two days scenario to forecast the third day weather event.

This study has accomplished the contribution as the fuzzy rule-based system is being implemented successfully in Matlab to perform weather event forecasting. Precision, reliability and consistency have been improved in order to determine and analyze meteorological forecasts. This also suggests that on the weather forecasting data a fuzzy inference method can be implemented as well. It is indeed evident from the result that the fuzzy method of inference is an effective climate modeling technique. A weather forecasting system can be developed by FRBS and the use of FIS can allow the user to produce a better outcome than the preceding one.

Although some techniques and concepts in forecasting weather events are a contribution to the paper, there are some modifications that should be introduced to boost potential efficiency in the future. These suggestions are to enhance the method that has been implemented in this work. The few aspects which need to be enhanced are the usage of data and parameters, the development of new effective techniques and many more.

ACKNOWLEDGEMENT

The authors would like to express their appreciation and gratitude to the Research Management Centre, Universiti Malaysia Sabah for the continued support.

REFERENCES

Agboola, A, & Gabriel. 2013.Development of a Fuzzy Logic Based Rainfall Prediction Model. International Journal of Engineering and Technology, vol. 3, no. 4, 427–435.

Awan, M. S. K. & Awais, M. M. 2011. Predicting Weather Events Using Fuzzy Rule-Based System. Applied Soft Computing, **11(1)**, 56–63.

Cihan, P. Fuzzy Rule-Based System for Predicting Daily Case in COVID-19 Outbreak. 2020. *4th International Symposium on Multidisciplinary Studies and Innovative Technologies (ISMSIT)*, Istanbul, Turkey, 2020, pp. 1-4, doi: 10.1109/ISMSIT50672.2020.9254714.

Hemayatkar, N., Khalili-Damghani, K., Didehkhani, H., & Samiee, R. 2018. Developing a fuzzy inference system to devise proper business strategies: A study on carpet industry. Journal of Industrial Engineering International, **15(3)**, 529–544.

Khatua, A., Jana, S., & Kar, T. K. 2020. A fuzzy rule-based model to assess the effects of global warming, pollution and harvesting on the production of Hilsa fishes. Ecological Informatics, 57(February), 101070. 1-7.

Malaysia Meteorological Department (MMD). 2016. General Climate of Malaysia (http://www.met.gov.my).

Mojiol, A. R. 2006. Ecological Landuse Planning and Sustainable Management of Urban and Sub-urban Green Areas in Kota Kinabalu, Malaysia. Goettingen: Cuvillier Verlag.

Moler, C., & Little, J. 2020. A history of MATLAB. Proceedings of the ACM on Programming Languages, 4(HOPL), 1–67.

Ross, T. J. 2010. Fuzzy Logic with Engineering Applications, 3rd Ed. John Wiley & Sons, Ltd.

Sharma, M., Mathew, L., & Chatterji, S. 2014. Weather Forecasting using Soft Computing and Statistical Techniques. International Journal of Advanced Research in Electrical, Electronics and Instrumentation Engineering, **3(7),** 11285–11290.

Zadeh, L.A. 1975. The Concept of a Linguistic Variable and Its Application to Approximate Reasoning-III. Information Sciences, vol. 9, no. 1, 43–80.

BorneoScience
The Journal of Science & Technology
Online ISSN : 2231-9085 | ISSN : 1394-4339

DESCRIPTIVE STATISTICAL CALIBRATION METHOD OF TRIAXIAL DIGITAL ACCELEROMETER ADXL345 AS EARTHQUAKES SENSOR

Nur Nazleen Johari[1], Chee Fuei Pien[1], Siti Rahayu Mohd Hashim[2], Bailon Golutin[3] & Jedol Dayou*[1]

[1] Energy, Vibration and Sound Research Group (e-VIBS), Faculty of Science and Natural Resources, Universiti Malaysia Sabah, Jalan UMS, 88400 Kota Kinabalu, Sabah, MALAYSIA.
[2] Mathematics with Economy Programme, Faculty of Science and Natural Resources, Universiti Malaysia Sabah, Jalan UMS, 88400 Kota Kinabalu, Sabah, MALAYSIA.
[3] Department of Mineral and Geoscience Sabah, Locked Bag 2042, 88999 Kota Kinabalu, Sabah, MALAYSIA.

*Corresponding author. Email: jed@ums.edu.my; Tel: +6-088-320302; Fax: +6-088-435324.

Received 13th November 2021; accepted 8th February 2023
Available online 20th April 2023
Doi: https: https://doi.org/10.51200/bsj.v44i1.4340

ABSTRACT: *Seismic monitoring networks are the crucial elements in strong motion seismology for effective risk reduction. Low scale lateral variation of high intensity ground movement caused by earthquakes will be detected more effectively with densely located networks. However, the limitations of developing such project are rooted in expensive costs associated with the construction and installation in addition to bulky size of the conventional seismic observation system. Recently, micro-electromechanical system (MEMS) has being recognized in the applications of seismological and earthquake engineering due to the high precision obtained in these micron size semiconductor instruments and cheaper alternative for traditional seismic detector. ADXL345 is a type of digital triaxial MEMS accelerometer that is ideal for measurement of low-frequency vibrations and static accelerations of gravity, which makes it suitable for ground motion detection. Thus, this study aims at calibrating ADXL345 sensor that is required as sensing component in an affordable earthquake monitoring system with the Earthquake Benchmarking System (Penanda Aras Gempa Bumi, PAG) available in the inventory of Department of Mineral and Geoscience Malaysia, Sabah. Soil vibrations in EW (east-west or x-axis), NS (north-south or y-axis), and UD (up-down or z-axis) directions during random forces hit on the surface are recorded by both accelerometers. Acceleration magnitudes recorded by PAG and ADXL345 are extracted and data exploration is performed. Predominantly, ADXL345 measurements in horizontal and vertical ground movements are on a higher scale than the reference device. Subsequently, evaluation by using descriptive statistical analysis is chosen to produce numerical equations for data correction operations. İmplementation of the mathematical functions in ADXL345 for observing land movements in EW, NS, and UD directions resulted in decreasing the range values of output readings. Higher approximation of magnitudes of ground motion with the PAG system is achieved.*

KEYWORDS. affordable, ground motion, calibration, descriptive analysis

INTRODUCTION

Propagation of seismic waves is due to the formation of earthquakes that result from the fault movement between tectonic plates (Jena and Pradhan, 2018). Gravitational and inertial forces from the quake generate ground movements causing lateral displacement of large shallow blocks of soils. Consequently, destructive effects are experienced in the faulted areas and increase the risk (Khoiry *et al.*, 2018) of life loss in the aftermath of demolition of buildings as well infrastructures (Khoiry *et al.*, 2018).

In a situation of a ravaging earthquake strikes an area, emergency rescue operations are facing crucial situations to save lives. The possibility of saving victims trapped or injured in a collapsed structure decreases exponentially as a function of time and eventually vanishes after hours (D'alessandro *et al.*, 2018). With massive seismic monitoring networks, low intensity lateral variation of land motion due to tremors will be measured effectively. This increases preparedness time prior to earthquake occurrence in a community and improve the efficiency of emergency management. However, the growth of seismic observation weakens as such projects can cost millions of dollars (Strauss and Allen, 2019) and usually heavy and bulky (Scudero *et al.*, 2018) with complex maintenance procedures. For instance, a complete seismic monitoring system for the West Coast of the United States would cost 16.1 million dollars per year and cost to increase number of stations as well to upgrade the system is 38 million dollars (Strauss and Allen, 2019).

Great advancements in seismological and earthquake engineering have been attained in the last decades following the technical modernization of the instrumentation. The quake monitoring application substantially developed in the 1990s in view of the introduction of MEMS (micro-electromechanical system) technology (Scudero *et al.*, 2018). MEMS device own its recognition as an affordable alternative of conventional earthquake detector, it is a high-precision system (Tanırcan *et al.*, 2017) with sensitivity and dynamic range that allows the measurement of earthquake obtained from a dimension on the order of microns (D'Alessandro *et al.*, 2014). Moreover, frequency response of a MEMS accelerometer can easily be improved by equalization (Sigcha *et al.*, 2018).

Triaxial Digital Accelerometer ADXL345 (ADXL345) is a type of MEMS accelerometer that is well suited for mobile device application. The measurement range of ADXL345 is ±2g to ±16g. The accelerometer sensor module able to record static acceleration of gravity in tilt-sensing application also dynamic acceleration from motion or shock. High resolution of ADXL345 scale range capable of detecting changes of inclination less than 1.0° (Description and Diagram, 2009). Physical properties of ADXL345 make it as ideal transducer module in the construction of seismic monitoring network. Hence, this research aims at calibrating ADXL345 accelerometer sensor that is required as sensing component in an affordable earthquake monitoring system with the Earthquake Benchmarking System (Penanda Aras Gempa Bumi, PAG) available in the inventory of Department of Mineral and Geoscience Malaysia, Sabah.

MATERIALS AND METHODS

In the process of calibrating ADXL345 with PAG as reference instrument, there are two major steps that are included which is the measurements of gravity acceleration in the field and the descriptive statistical calibration that is performed on the data obtained. ADXL345 device (in Figure 1) used for seismic data acquisition was built by integrating the accelerometer sensor module with processing unit which is the Arduino Mega 2560 microcontroller.

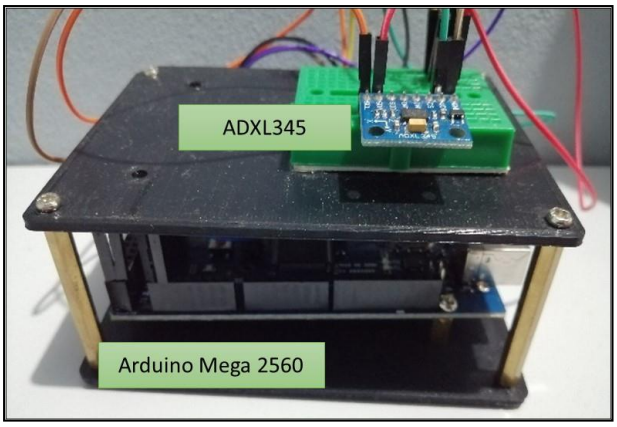

a. Photo of the sensing instruments

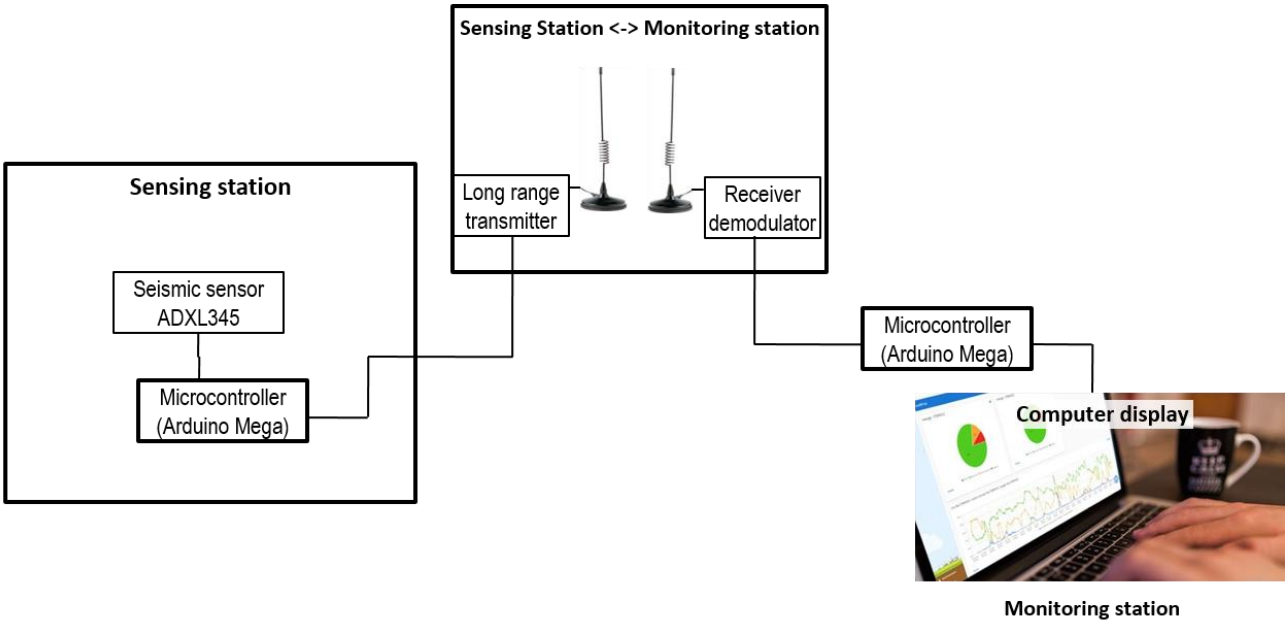

b. Complete block diagram of the earthquake measurement system using ADXL345

Figure 1: ADXL345 earthquake sensor consists of ADXL345 triaxial digital accelerometer, and Arduino Mega 2560 microcontroller as the processing unit

Field tests are conducted by creating a simulation of an earthquake condition in an outdoor area. ADXL345 device and PAG is placed 1.0 m from each other as shown in Figure 2. Hit forces randomly given to the ground surface using a hammer at a distance of 3.0 m from both systems to mimic the propagation of seismic waves. Ground acceleration in the direction of EW (east-west or also known as x-axis), NS (north-south or y-axis), and UD (up-down or z-axis) is recorded simultaneously by ADXL345 and PAG. Then, acceleration magnitudes are extracted to perform data exploration. Next, linear regression analysis is performed using SPSS (Statistical Package for the Social Sciences) to obtain the correlation coefficient (R) of recorded data by both devices. By using descriptive statistical calibration method, numeral equations are formed for data correction operation.

Figure 2: Placement of PAG and ADXL345 is in distance 1.0m and force is given from 3.0m away of both devices.

RESULTS AND DISCUSSION

Measurements of ground acceleration obtained from PAG and ADXL345 system in the directions of EW, NS, and UD due to impact force on surface of the ground plotted in line graphs as presented in Figure 3. It can be seen there is huge difference between the two recorded data. Linear regression analysis of raw data of ADXL345 and the reference instrument (in Figure 4) in the direction of EW, NS, and UD resulted in R values of 0.364, 0.562, and 0.306, respectively. The correlation coefficient indicates a low positive correlation (Mukaka, 2012) between the MEMS accelerometer sensor and the reference instrument.

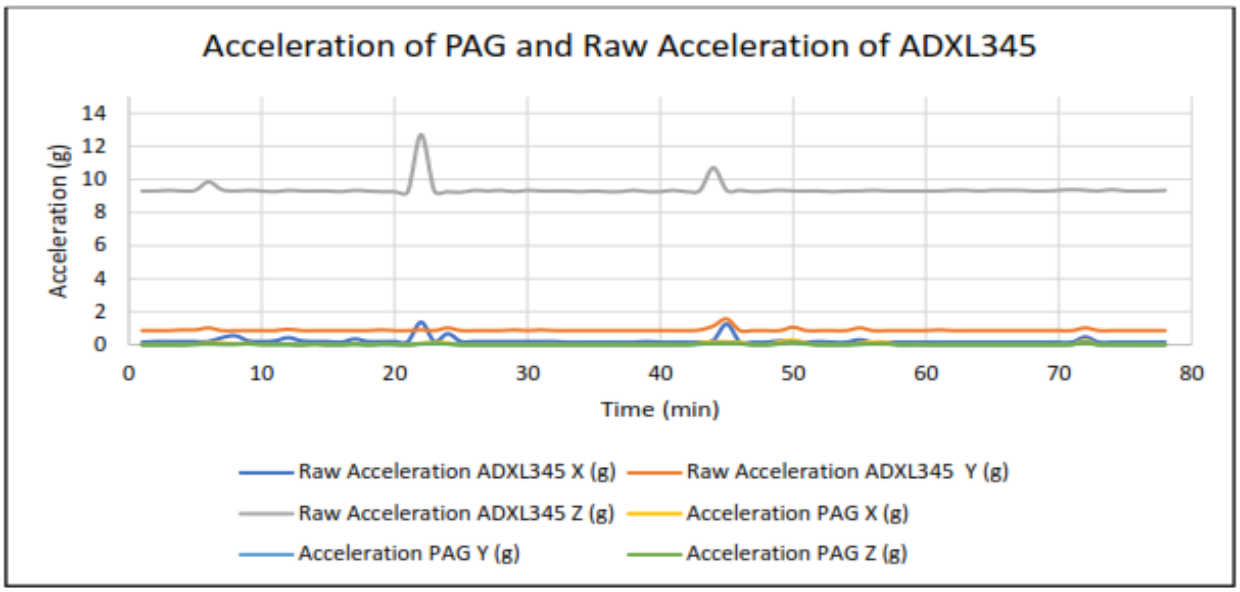

Figure 3: Line graph plots of the ground acceleration obtained using ADXL345 and PAG in directions of EW (x), NS (y), and UD (z)

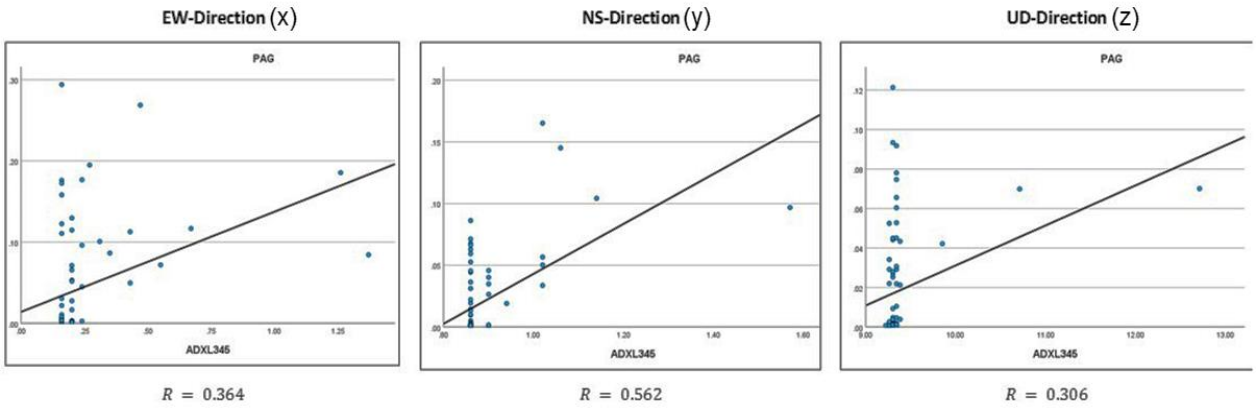

Figure 4: Linear regression of raw acceleration readings from ADXL345 and PAG for each orientation of motion.

Detail examination shows that ADXL345 recorded higher value of soil motion in horizontal (EW and NS) and vertical (UD) axis compared to readings from PAG (Figure 3). The overall recorded data are in the range of 0.00 g to 0.29 g for PAG and 0.16 g to 12.67 g for ADXL345. Therefore, a correction to the observed data should be carried out and is described in the following.

The descriptive statistical calibration method is performed by observing the mean of acceleration on sensitive axis of ADXL345 within the scale range measured in the relative axis by PAG. Sensitive axis of ADXL345 by mean is the axis that succeeded to respond and measured corresponding either increase or decrease pattern on motion of relative axis recorded by PAG. Calculation of correction factor is performed for the average data from sensitive axis on ADXL345 with readings on the similar axis of PAG. Correction factor for the other axis is calculated from the average calibrated data of sensitive axis of ADXL345 with mean of relative data on the remaining axis of PAG. Subsequently, numeral equations are formed by including the correction factors for correcting the data of the MEMS device. Mathematical functions for producing data in ranges of 0.00 g to 0.29 g on ADXL345 are listed in Table 1. In those equations, $x, y,$ and $z,$ is the average raw data and $X, Y,$ and Z is the mean calibrated data of axis EW, NS, and UD respectively.

Table 1: Numeral Equations Formed to Calibrate Data Obtained From ADXL345.

Range	Sensitive Axis on ADXL345	Equation
0.00g – 0.09g	UD or Z-Axis	$Z = z\ v?\ 233.4$
		$X = Z \times 2.72$
		$Y = Z \times 1.34$
0.10g – 0.19g	NS or Y-Axis	$Y = y\ v?\ 7.31$
		$X = Y \times 2.03$
		$Z = Y\ v?\ 1.20$
0.20g – 0.29g	EW or X-Axis	$X = x\ v?\ 1.75$
		$Y = X\ v?\ 1.63$
		$Z = X\ v?\ 2.93$

Implementation of the numeral functions in ADXL345 described in Table 1 has lowered its measurement range values close to that of PAG. The linear regression analysis made for the calibrated data

EW, NS, and UD, respectively. These values are much higher compared to the correlation in the original data shown in Figure 4. This indicates that the data of ADXL345 now has a high positive correlation (Mukaka, 2012) and better represents the observed data from ADXL345 in comparison with the reference measurement using PAG. This is shown in Figure 6 where there is huge improvement between the data acquired using numerically calibrated ADXL345 and from PAG, in comparison before the calibration shown in Figure 3.

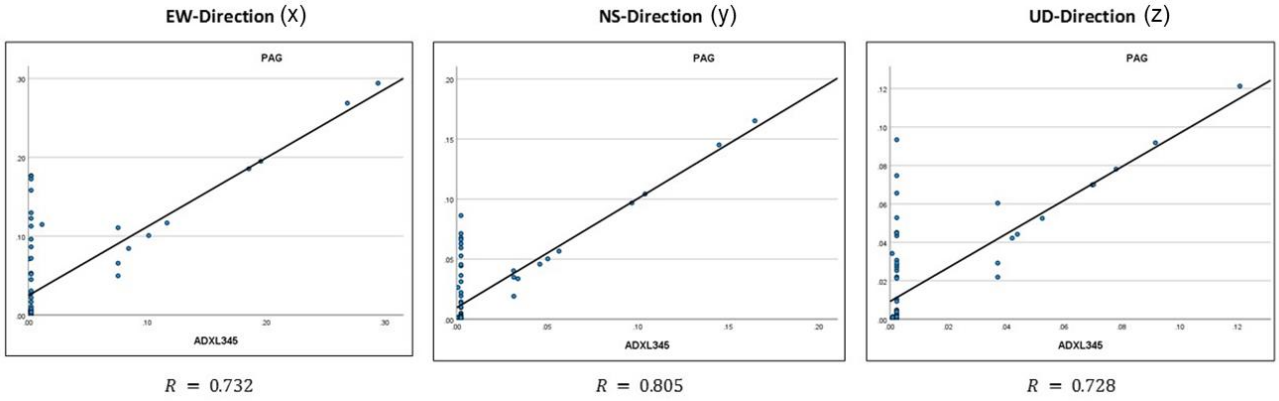

Figure 5: Linear regression analysis of calibrated data ADXL345 and PAG for each direction of motion EW, NS, and UD

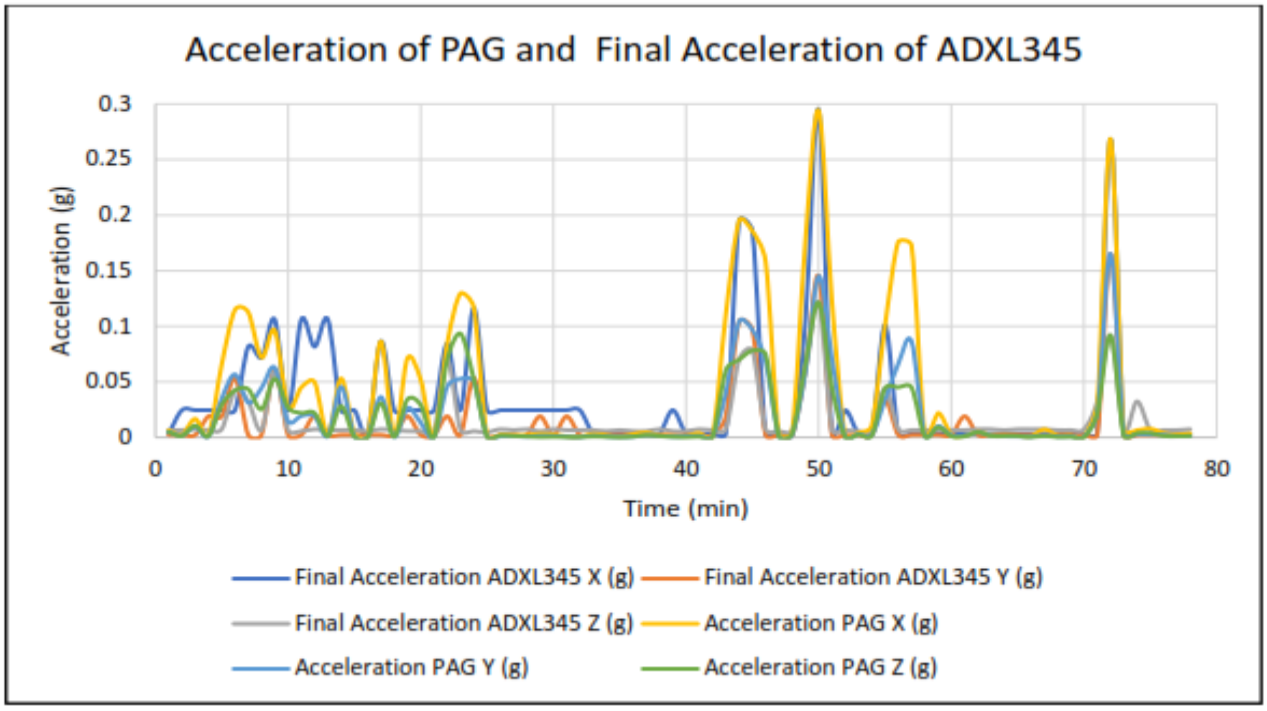

Figure 6: Graphical comparison of the readings from ADXL345 and PAG with simulated ground acceleration (refer Figure 2 for simulating ground acceleration using a hammer).

CONCLUSION

Calibration of ADXL345 earthquake sensor with the reference instrument PAG was conducted using descriptive statistical calibration method. Mathematical equalizations are produced by calculating multiplication factors on average range data on sensitive axis of ADXL345 relative to the mean of average of respond data on PAG. Corrected data after the implementation of numeral equations for each range and

has decreased the range scale of measured data on ADXL345 and consequently increased the correlation coefficient between the accelerometer sensor and PAG. This has highly improved the accuracy of displayed data from ADXL345 and is ready to be integrated in a construction of actual seismic monitoring networks.

ACKNOWLEDGEMENT

Collaboration of Department of Mineral and Geoscience Malaysia, Sabah and fund from UMSGreat GUG0334-1/2019 in this research is greatly acknowledged.

REFERENCES

D'alessandro, A., D'anna, R., Greco, L., Passafiume, G., Scudero, S., Speciale, S., & Vitale, G. (2018). Monitoring Earthquake through MEMS Sensors (MEMS project) in the town of Acireale (Italy). *5th IEEE International Symposium on Inertial Sensors and Systems, INERTIAL 2018 - Proceedings*, 1–4. https://doi.org/10.1109/ISISS.2018.8358143.

D'Alessandro, A., Luzio, D. & D'Anna, G. (2014). Urban MEMS based seismic network for post-earthquakes rapid disaster assessment. *Advances in Geosciences*, **40**, 1–9. https://doi.org/10.5194/adgeo-40-1-2014.

Analog Devices. (2009). *Digital Accelerometer: Data Sheet ADXL345*. https://www.analog.com/media/en/technical-documentation/data-sheets/ADXL345-EP.pdf.

Jena, R., & Pradhan, B. (2018). A novel model for comparing Peak Ground Acceleration derived from three attenuation laws using an integrated GIS technique in Sabah area, Malaysia. *International Journal of Scientific and Research Publications*, **8**(9), 191–200. https://doi.org/10.29322/IJSRP.8.9.2018.p8127.

Khoiry, M. A., Hamzah, N., Osman, S. A., Mutalib, A. A. & Hamid, R. (2018). Physical Damages Effect on Residential Houses Caused by the Earthquake at Ranau, Sabah Malaysia. *International Journal of Engineering and Technology*, **10**(5), 414 - 418. https://doi.org/10.7763/IJET.2018.V10.1094.

Mukaka, M. M. (2012). Statistics Corner : A guide to appropriate use of Correlation coefficient in medical research. *Malawi Medical Journal*, **24**(3), 69–71.

Scudero, S., D'Alessandro, A., Greco, L. & Vitale, G. (2018). MEMS technology in seismology: A short review. *2018 IEEE International Conference on Environmental Engineering, EE 2018 - Proceedings*, 1–5. https://doi.org/10.1109/EE1.2018.8385252.

Sigcha, L., Pavón, I., Arezes, P., Costa, N., De Arcas, G. & López, J. M. (2018). Occupational risk prevention through smartwatches: Precision and uncertainty effects of the built-in accelerometer. *Sensors (Switzerland)*, **18**(11): 1–20. https://doi.org/10.3390/s18113805.

Strauss, J. A. & Allen, R. M. (2019). Benefits and Costs of Earthquake Early Warning. *Seismological Research Letters*, **87**(3): 765–772. https://doi.org/10.1785/0220150149.

Tanırcan, G., Alçık, H. & Beyen, K. (2017). Reliability of MEMS accelerometers for instrumental intensity mapping of earthquakes. *Annals of Geophysics*, **60**(6): SE673. https://doi.org/10.4401/ag-7501.

BorneoScience
The Journal of Science & Technology
Volume 44 Issue 1 : April 2023
Online ISSN : 2231-9085 | ISSN : 1394-4339

MINERALOGICAL AND GEOCHEMICAL STUDY OF ANDESITE ALTERATION ZONE IN BUKIT MANTRI GOLD MINE, BALUNG, SABAH

Mohd Shafreen Mad Isa[1] and Baba Musta[2]

[1, 2] Faculty of Science and Natural Resources,
University Malaysia Sabah, Malaysia, Jalan UMS, 88400 Kota Kinabalu, Sabah, Malaysia

Email: shafreen@live.com.my[1], babamus@ums.edu.my[2]

Received 09th September 2022; accepted 8th February 2023
Available online 20th April 2023
Doi: https://doi.org/10.51200/bsj.v44i1.4347

ABSTRACT: *This paper highlights the geochemical compositions and mineralogy of the alteration zone of the andesitic host rock and volcanic breccia in Bukit Mantri area near Balung, Tawau, Sabah, where a gold mining project is now taking place. Minerals identified by XRD analysis include quartz, pyrite, K-feldspar, muscovite, chlorite, kaolinite, hematite, and goethite, while thin section analysis confirms the abundance of pyrite. XRF and ICP-OES analyses suggest a significant concentration of SO_3, Cu, Pb, Zn and As, with average values of 2.68wt%, 254µg/g, 236.9µg/g, 232.9µg/g, and 30.6µg/g, respectively, in the hydrothermally altered andesite. The widespread presence of pyrite and higher concentration of SO_3 provide insights for environmental control for its higher acidity generation potential. Meanwhile, secondary minerals such as iron and aluminium oxides and silicate minerals may provide acid buffers and reduce the dispersion of constituents.*

KEYWORDs: geochemistry, mineralogy, hydrothermal alterations, gold mineralisation, Bukit Mantri

INTRODUCTION

A mining lease was issued for a gold mining project in 2013 and began developing its mine between 2017 and 2018 in Bukit Mantri, near Balung, Tawau, Sabah. The approved mining lease is situated between Bukit Mantri and Bukit Tundong, geographically bounded by 4°29'N to 4°31'N and 118°6'E to 118°8'E, near Balung, Tawau, Sabah (Figure 1). The first phase of mine development and mining activities focuses on the Bukit Mantri area.

The geology of the area is characterised by andesitic to dacitic volcanic flow and pyroclastic of Pliocene, and Kalumpang Formation, which consists of marine sediments interbedded with volcaniclastics composed of tuff, sandstone, claystone, volcanic conglomerates and breccia, and limestone, and deposited in an early Middle Miocene shallow neritic environment (Musta et al., 2008; Tahir et al., 2010).

The volcanic hosts an epithermal low-sulphidation gold deposit (Haruna, 2016; Yan, 1991), and the mineralisation is described as a series of quartz-sulphide hydrothermal breccia veins enveloped by quartz-adularia-sericite near the veins, argillic, and propylitic alterations. Other reported alteration profiles include silicic, late-stage kaolinitic, and late-stage carbonate. These wall-rock alterations indicate the changes in geochemical composition and mineralogy of host rock (Nordstrom, 2011) and potentially affect the surrounding environment as they both can increase and decrease acid-generating capacity (Plumlee, 1999).

Moreover, oxidations, formation of secondary minerals and sorption could also superimpose the variability of the geochemical composition of the mineral deposits and host rocks (Nordstrom & Alpers, 1999; Plumlee, 1999; Smith, 1999).

Presently, the background geochemical composition and mineralisation, and their relationship to hydrothermal mineralisation and dispersion, are unavailable. Therefore, the objectives of this study are to examine the geochemical composition of hydrothermally altered host rocks and volcanic breccia in the area and to discover signature minerals that may have an impact on the environment.

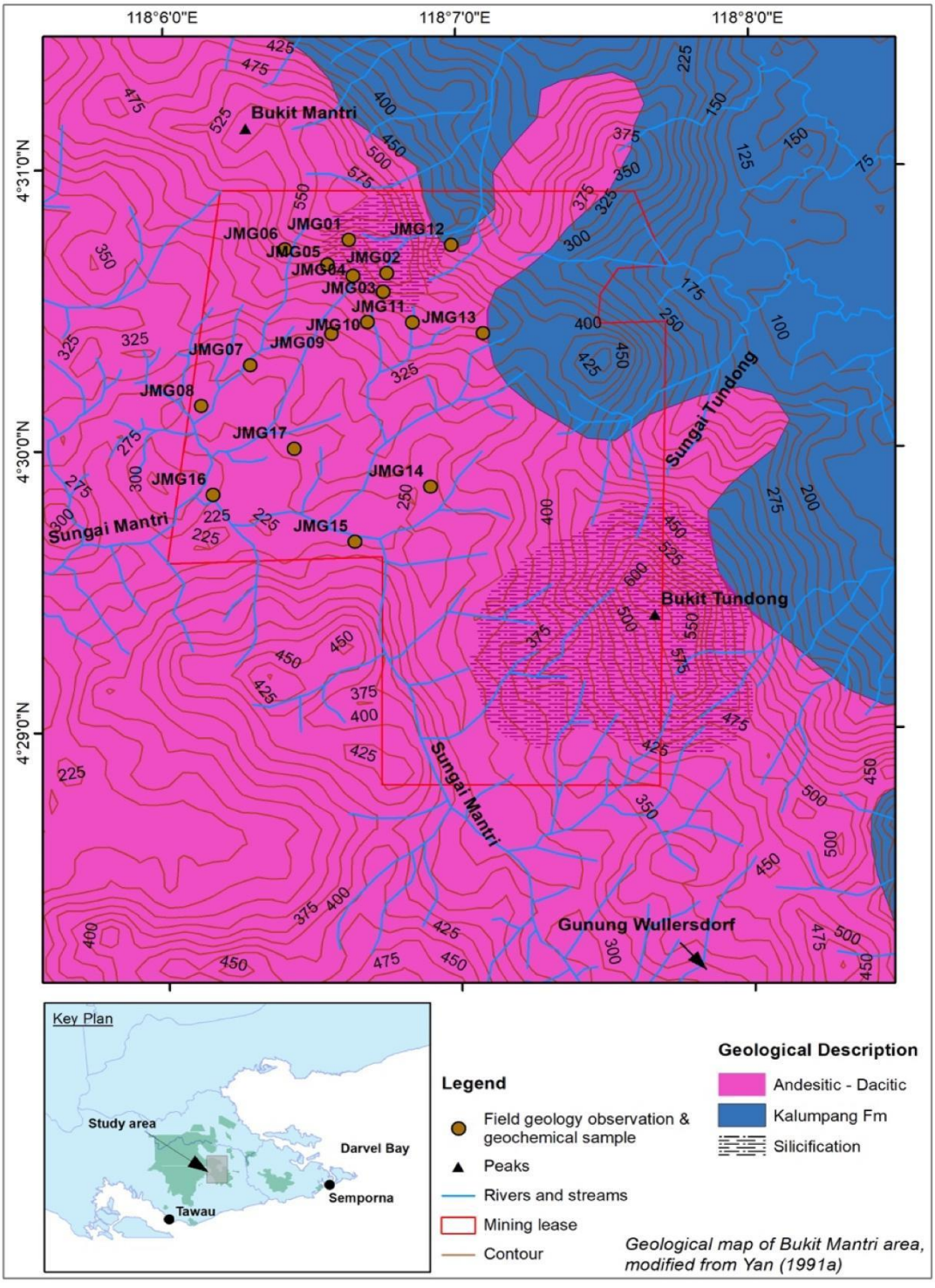

Figure 1. The geological map of the study area based on Yan (1991) and the distribution of sampling locations.

MATERIALS AND METHODS

Seventeen hand specimen samples of the alteration zone of andesitic rock were collected from fresh outcrops in the surrounding area of Bukit Mantri during the early phase of mine development in May 2018 (Figure 2), and they are identified as argillised, propylitised, silicified, argilised and sulphidised andesite, and volcanic breccia. The descriptions of the hand specimens are listed in Table 1.

Selected hand specimens of argilised, propylitised and silicified andesite were cut, placed on glass, and polished to a thickness of about 0.03 mm for thin section analysis (Figure 3), and the identification of minerals is based on Mackenzie et al. (2017). Meanwhile, crushed and pulverised samples were then used for mineral identification by X-Ray Diffraction (XRD) technique using Cu-source X-Ray, measuring at diffraction angle, 2θ between 10° and 80° for about 30 minutes using Bruker D8 Advance (Bruker Corp.), subsequently analysed using High Score Plus Version 3.0.5 application (Malvern Panalaytical Inc.) with The American Mineralogist Crystal Structure Database as the reference (Clark & Downs, 2004; Downs & Hall-Wallace, 2003).

Major elements geochemistry was analysed using pre-prepared fuse discs from the pulverised samples with X-Ray Fluorescence (XRF) Spectrometer (Musta et al., 2008) using PANAnalytical Zetium XRF Spectrometer (Malvern Pananalytical Inc.). In contrast, trace elements were measured using Inductively Coupled Plasma - Optical Emission Spectrometry (ICP-OES) technique using Perkin Elmer Optima 5300 DV Spectrometer (PerkinElmer Inc.). Prior to ICP-OES analysis, samples were digested with 70% concentrated HNO_3 and 50% concentrated HF inside Teflon beakers under slow heating between 90°C and 100°C on a hotplate. Loss on Ignition (LOI) was performed gravimetrically and incorporated for the total of major elements geochemistry calculation. General statistical and coefficient of correlation analysis (r) calculations were performed in Microsoft Excel 365 (Microsoft Corp.).

Figure 2. Outcrops and hand specimen samples in the alteration zone of andesite and volcanic breccia in Bukit Mantri area; (a) and (b) argillised andesite, (c) and (d) propylitised andesite, (e) and (f) silicified andesite, (g) and (h) volcanic breccia, and (i) and (j) argillised and sulphidised andesite.

Table 1. Description of hand specimens of hydrothermally altered andesite and volcanic breccia in Bukit Mantri área

ID	Description of hand specimen	ID	Description of hand specimen
JMG-01	Weak to moderately argillised andesite, yellowish — purplish dark brown, moderate to highly oxidised and weathered, moderately limonitic, ferromanganese (Fe-Mn) was observed in some parts, mostly along with the fractures, and no sulphides were noted.	JMG-02	Weakly argillised andesite, yellowish — purplish dark brown, moderate to highly oxidised and weathered, moderately limonitic with few ferromanganeses (Fe-Mn) along the fractures, cut by weak — moderately intense quartz veinlets, and disseminated relics of fine-grained sulphides observed most likely pyrite.
JMG-03	Moderately argillised andesite. Whitish to yellowish, highly oxidised and weathered, moderately limonitic with few ferromanganeses (Fe-Mn) along the fractures, relics of fine-grained pyrite observed in some parts .	JMG-04	Moderate to highly argilllised andesite, whitish to purplish, highly oxidised and weathered, moderately limonitic, moderately cut by quartz veins.
JMG-05	Prophylitic andesite, slightly weathered to fresh, greenish grey, moderate to strongly chloritised, cut by few limonitic quartz veins, dissemination of fine-grained pyrite and few chalcopyrite observed pervasively.	JMG-06	Prophylitic andesite, slightly weathered to fresh, greenish grey, porphyritic with phenocryst of feldspar, weak to moderately chloritised, dissemination of fine-grained pyrite noted.
JMG-07	Moderate to highly weathered and oxidised andesite, purplish to whitish-yellow, moderately argilised, limonite observed mostly along fractures, pyrite relics noted in some parts.	JMG-08	Moderate to highly weathered and oxidised andesite, yellowish to purplish brown, weak to moderately limonitic and hematitic mostly along fractures, relics of sulphides noted in some parts.
JMG-11	Moderate to strongly argillised andesite, whitish - greenish grey, chloritic, moderately to highly oxidised and weathered, moderately limonitic with the dissemination of fine-grained pyrite observed.	JMG-12	Volcanic breccia/Volcanoclastic with angular to subangular volcanic rock clasts, yellowish to reddish-brown, highly weathered and oxidised, cut by weakly intense ferromanganese (Fe-Mn) veins, no sulphides observed.
JMG-13	Highly weathered and oxidised propylitised andesite, yellowish to purplish brown, clayey, cut by weakly intense ferromanganese (Fe-Mn) veins, no sulphides observed.	JMG-14	Moderate to highly sulphidised and argillised andesite, highly weathered and oxidised, greenish – whitish light grey, dissemination of fine to medium-grained pyrite observed pervasively.

ID	Description of hand specimen	ID	Description of hand specimen
JMG-15	Moderate to highly sulphidised and argilised Andesite, moderately to highly weathered and oxidised, greenish — whitish light grey, disseminating fine to medium-grained pyrite observed pervasively.	JMG-16	Moderate to highly sulphidised and argilised andesite, greenish — whitish light grey, moderately to highly weathered and oxidised, cut by weak to moderately intense limonitic quartz veins, dissemination of fine to medium-grained pyrite observed pervasively.
JMG-17	Moderate to highly sulphidised and argilised andesite, greenish — whitish light grey, moderately to highly weathered and oxidised, limonitic quartz veins noted in few parts, dissemination of fine to medium-grained pyrite observed pervasively.		

RESULTS & DISCUSSION

Mineralogy

Quartz, pyrite, muscovite, K-feldspar, chlorite, goethite, hematite, and kaolinite are minerals that appear in XRD spectrograms (Figure 4). Pyrite becomes a major mineral after quartz, appearing in argillised, propylitised, silicified, sulphidised and argillised andesite. Muscovite is found in sulphidised and argillised andesite, whereas K-feldspar and chlorite are identified in propylitised andesite. Additionally, goethite, hematite, and kaolinite are also presented, and these secondary minerals are the results of weathering on the country rocks.

The specimens' micrographs under plane-polarised light (PPL) and cross-polarised light (XPL) confirm the presence of quartz, pyrite, K-feldspar and chlorite (Figure 3). Pyrite has been observed in all specimens, including propylitised andesite, indicated by dark (opaque) and cubical-shaped crystals in the optical micrographs. Meanwhile, K-feldspar, chlorite, and mineral crystals of unidentified sulphide minerals that appeared alongside pyrite are observed in propylitic and argillised andesite, respectively. In the prospecting and earlier geochemical survey reports, some notable sulphide minerals are chalcopyrite, sphalerite and galena, while muscovite and K-feldspar are referred to as sericite and adularia, respectively (Haruna, 2016; Yan, 1991). The analyses on XRD spectrograms and thin section microscopy suggest that pyrite is highly distributed in host rocks and has become the principal mineral of environmental concern owing to its potential to increase acid-producing capacity. Meanwhile, the availability of silicate and secondary minerals in the area could attenuate acid waters and limit trace elements' mobility.

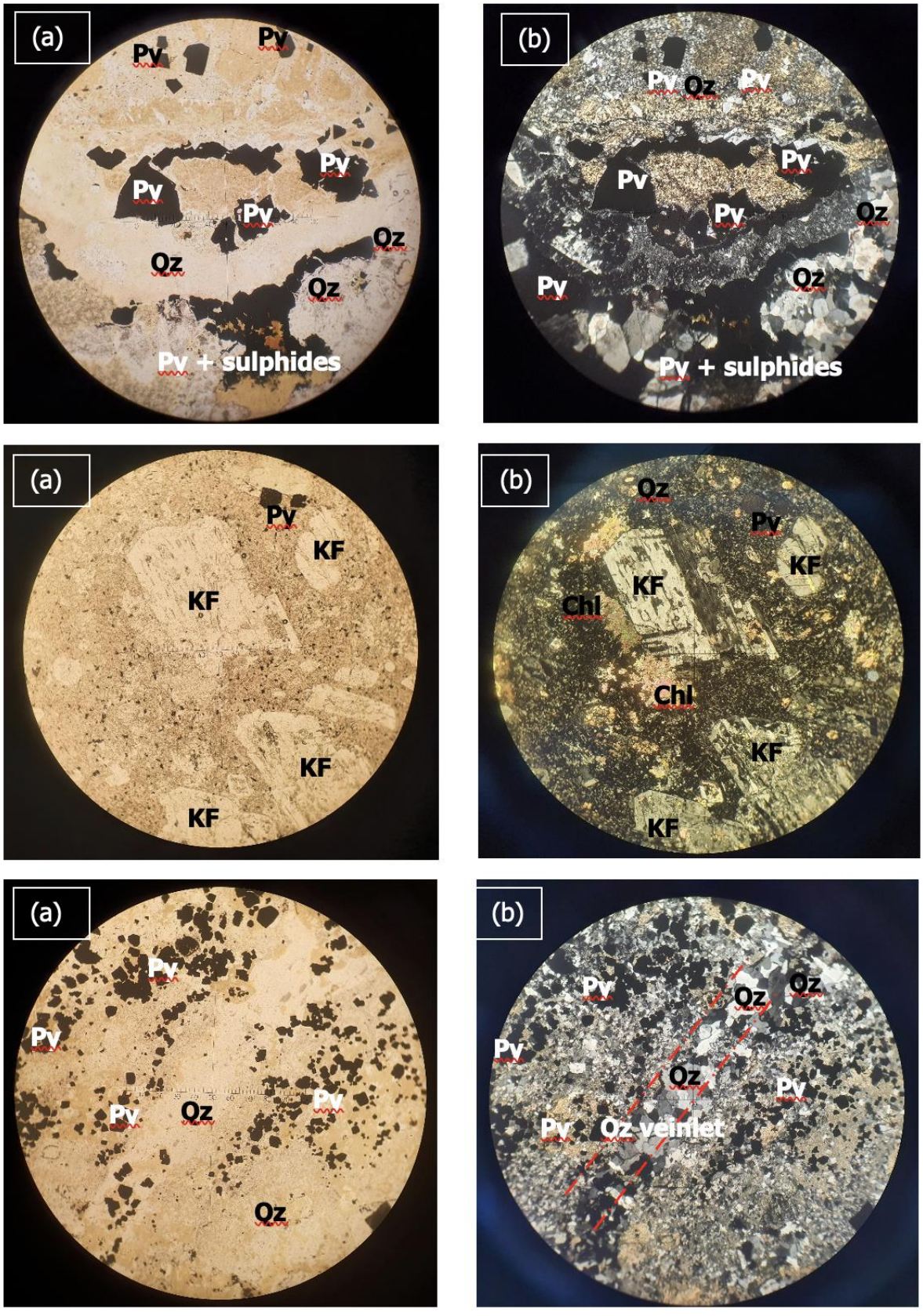

Figure 3. Thin section optical microscopy images of selected hydrothermally altered andesite; (a) argillised andesite (PPL), (b) argilised andesite (XPL), (c) propylitised andesite (PPL), (d) propylitised andesite (XPL), (e) silicified andesite (PPL), and (f) silicified andesite (XPL), showing the presence of quartz (Qz), pyrite (py), K-feldspar (KF), and chlorite (Chl).

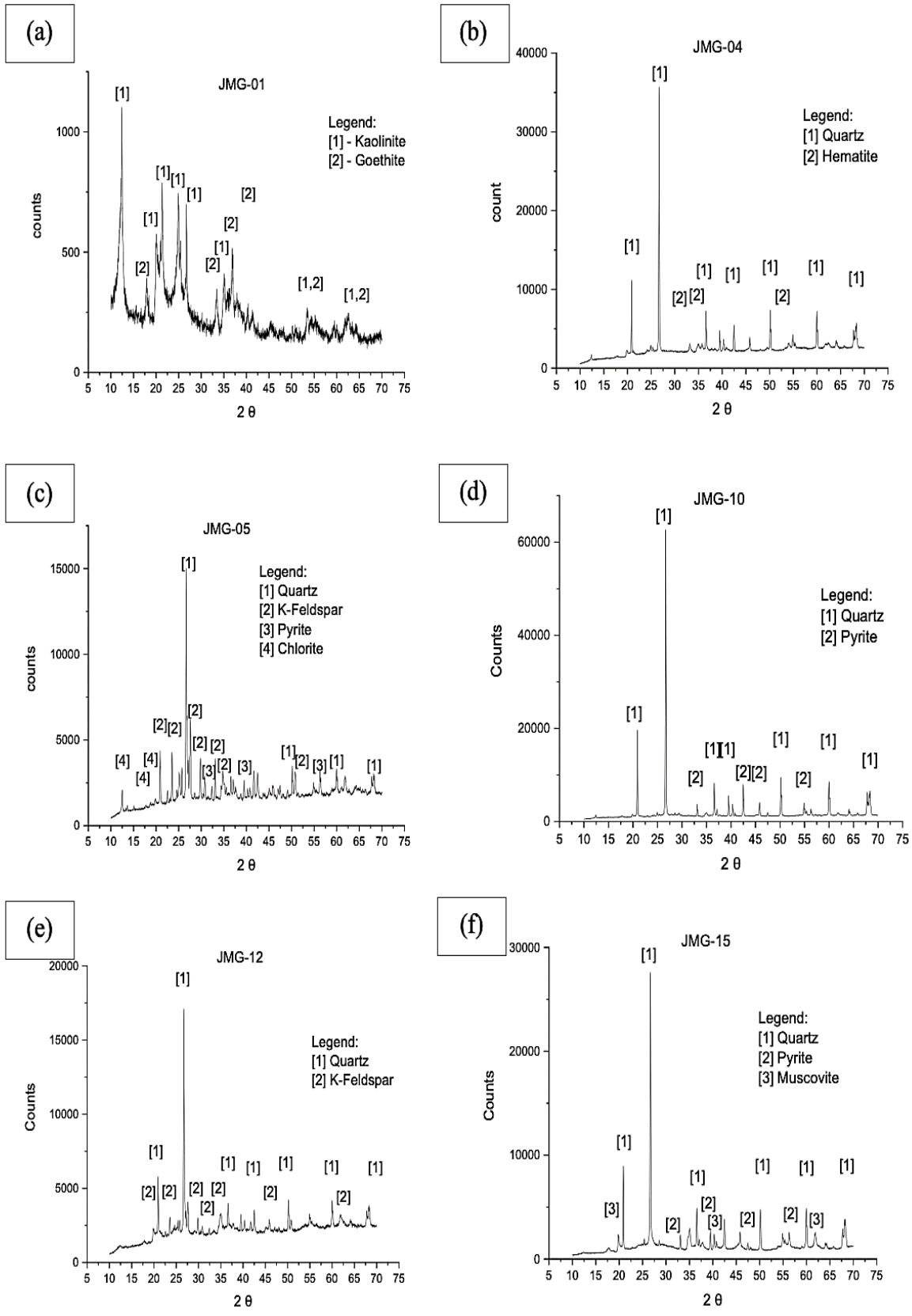

\

Figure 4. XRD Spectrograms show mineral phases identified as [a] kaolinite and goethite in highly weathered argilised andesite, [b] quartz and hematite in weathered argilised andesite, [c] quartz, K-feldspar, pyrite, and chlorite in propylitised andesite, [d] quartz and pyrite in silicified andesite, [e] quartz and K-feldspar in volcanic breccia, and [f] quartz, pyrite, and muscovite in sulphidised and argilised andesite.

Major elements geochemistry

Tables 2 and 3 summarise the results of major element geochemistry and the calculation results of coefficient of correlations among the major elements. SiO_2 is the most abundant oxide in the country rocks, ranging from 32.77wt% to 74.39wt%. Al_2O_3 and $Fe_2O_3^T$ are the second and third most abundant oxides, between 6.11wt% and 26.00wt%, 3.73wt% and 23.45wt%, respectively. The oxide of other major elements such as TiO_2, K_2O, MnO, MgO, CaO, Na_2O and P_2O_5 made up the rest of the geochemical compositions, from below the detection limit to 7.52wt%. Meanwhile, SO_3 is ranging 0.03wt% to 7.35wt%, and LOI from 3.28wt% to 13.45wt%.

Silicified andesite has the most SiO_2. During silicification, rock materials have been replaced by SiO_2 (Plumlee, 1999), resulting in a higher SiO_2 concentration. SiO_2 has a moderate to strong negative correlation with Al_2O_3 and $Fe_2O_3^T$ (r=-0.80 and r=-0.75), suggesting the formation of secondary minerals containing these oxides are likely to form as the degree of weathering increases while the concentration of SiO_2 decreases. The average $Fe_2O_3^T$ composition of all andesite samples is 8.56wt%, relatively higher than the reference composition, 3.27wt% (Winter, 2014), indicating that the country rock has relatively weathered.

The average concentration of MgO, CaO and Na_2O in the hydrothermally altered andesite are 1.03wt%, 0.09wt%, and 0.06wt%, respectively, which appear to be lower than their respective reference compositions of 3.33wt%, 6.79wt%, and 4.48wt%, whereas K_2O and MnO are 3.36wt% and 0.41wt%, respectively have increased from 1.62wt% and 0.14wt%. The near-zero correlation of MgO, CaO and Na_2O with Al_2O_3 and $Fe_2O_3^T$ suggests the leaching of these oxides during weathering is relatively weak but varying due to hydrothermal alterations. MgO and CaO are also relatively higher in propylitised andesite than in other alteration profiles of andesite and volcanic breccia. The relatively higher average of K_2O than the reference composition and the relatively higher concentration in propylitic andesite and volcanic breccia suggest hydrothermal alterations have introduced and enriched potassium-bearing minerals such as K-feldspar or adularia in the parent rocks.

Table 2. The concentration of major elements in hydrothermally altered andesite and volcanic breccia in Bukit Mantri gold mine area, Tawau, Sabah.

Id	Rock Type[alt.]	SiO_2	TiO_2	Al_2O_3	$Fe_2O_3^T$	MnO	MgO	CaO	Na_2O	K_2O	P_2O_5	SO_3	LOI	TOTAL
		wt%												
JMG-01	And.[arg.]	32.77	1.01	26.00	23.45	1.49	0.17	0.00	0.02	1.11	0.14	0.38	13.45	100.00
JMG-02	And.[arg.]	74.39	0.61	12.99	4.82	0.03	0.46	0.03	0.06	2.90	0.05	0.36	3.28	100.00
JMG-03	And.[arg.]	56.80	0.72	18.51	10.72	2.07	0.77	0.02	0.05	3.52	0.03	0.11	6.68	100.00
JMG-04	And.[arg.]	66.56	0.61	14.13	10.80	0.03	0.37	0.01	0.02	1.80	0.03	0.17	5.47	100.00
JMG-05	And.[prop.]	53.81	0.57	14.82	8.76	0.42	1.49	0.04	0.13	7.32	0.03	6.16	6.46	100.00
JMG-06	And.[prop.]	61.62	0.64	15.28	7.36	0.91	3.34	1.05	0.07	4.63	0.10	0.30	4.71	100.00
JMG-07	And.[arg.]	66.76	0.75	19.67	3.73	0.02	0.53	0.03	0.04	2.94	0.01	0.03	5.49	100.00
JMG-08	And.[prop.]	60.43	0.70	17.89	10.21	0.03	0.66	0.01	0.02	2.70	0.02	0.09	7.26	100.00
JMG-09	And.[arg.]	61.70	0.64	14.80	7.46	0.03	0.76	0.02	0.09	2.97	0.03	0.31	11.18	100.00
JMG-10	And.[si.]	74.14	0.20	6.11	6.34	0.04	0.13	0.04	0.01	1.14	0.02	6.06	5.77	100.00
JMG-11	And.[arg.]	55.04	0.83	17.98	10.51	0.26	1.57	0.06	0.14	3.04	0.10	3.53	6.96	100.00
JMG-12	Volc. Breccia	58.04	0.94	18.91	8.93	0.94	0.47	0.03	0.08	4.68	0.08	0.07	6.84	100.00
JMG-13	And.[prop.]	48.43	1.05	23.90	9.93	1.04	0.15	0.01	0.12	7.52	0.04	0.13	7.67	100.00
JMG-14	And.[arg., sulph.]	62.05	0.52	14.59	5.24	0.05	0.86	0.06	0.04	3.70	0.01	5.52	7.37	100.00
JMG-15	And.[arg., sulph.]	60.58	0.65	16.78	4.57	0.02	1.07	0.02	0.03	3.28	0.02	5.37	7.61	100.00
JMG-16	And.[arg., sulph.]	54.39	0.59	16.12	6.59	0.07	3.15	0.02	0.09	1.55	0.03	7.35	10.05	100.00
JMG-17	And.[arg., sulph.]	51.85	0.56	17.12	6.49	0.03	0.95	0.03	0.08	3.62	0.03	6.98	12.27	100.00
Minimum		32.77	0.20	6.11	3.73	0.02	0.13	0.00	0.01	1.11	0.01	0.03	3.28	
Maximum		74.39	1.05	26.00	23.45	2.07	3.34	1.05	0.14	7.52	0.14	7.35	13.45	
Average[1], x̄		58.83	0.67	16.67	8.56	0.41	1.03	0.09	0.06	3.36	0.04	2.68	7.61	
Ref. comp.		57.9	0.87	17.0	3.27	0.14	3.33	6.79	3.48	1.62				99.27[2]

Remarks: Alt = alteration, And = andesite, arg. = argilised, prop. = propylitised, si. = silicified, sulp. = sulphidised, bdl = below detection limit, Ref. comp. = ref composition. The geochemical compositions are normalised to 100 wt%. [1] = average exclude of volcanic breccia, [2] = include H_2O composition of 0.83%. Reference andesite geochemical composition: Winter (2014).

Table 3. The coefficient of correlations, r between major elements.

Item	TiO_2	Al_2O_3	$Fe_2O_3^T$	MnO	MgO	CaO	Na_2O	K_2O	P_2O_5	SO_3	LOI
SiO_2	-0.66	-0.80	-0.75	-0.55	-0.05	0.10	-0.28	-0.18	-0.55	-0.01	-0.74
TiO_2		0.93	0.55	0.55	-0.16	-0.08	0.31	0.32	0.55	-0.58	0.25
Al_2O_3			0.59	0.55	-0.13	-0.12	0.19	0.24	0.45	-0.41	0.45
$Fe_2O_3^T$				0.61	-0.23	-0.10	-0.09	-0.17	0.70	-0.33	0.49
MnO					-0.06	0.17	0.07	0.24	0.50	-0.43	0.12
MgO						0.65	0.37	0.07	0.16	0.33	-0.03
CaO							0.06	0.18	0.37	-0.16	-0.29
Na_2O								0.65	0.18	0.16	0.07
K_2O									-0.07	-0.05	-0.20
P_2O_5										-0.32	0.22
SO_3											0.24

SO_3 is consistently higher in argilised and sulphidised andesite, and its concentration is also significant in some argilised, propylitised and silicified andesite, whereas it is least in volcanic breccia. It is anticipated that the sulphidation process has fundamentally altered the geochemistry and increased the concentration of sulphide minerals, especially pyrite. LOI was found in high concentrations in the parent rocks. The coefficient of correlation between LOI and SiO_2 shows a negative and moderate relationship (r= -0.74), implying it also shows volatile matters such as sulphur gases in sulphidised samples are likely higher in weathered materials than in relatively fresh parent rocks.

Trace elements geochemistry

Results of ICP-OES on trace element geochemistry are tabulated in Table 4. The concentration of trace elements, i.e. As, Ba, Cu, Pb, Zn, Cd, Cr, Ni, and Ag are 8.1µg/g to 129.2µg/g, 101.0µg/g to 103.8µg/g, 9.1µg/g to 827.1µg/g, 12.2µg/g to 535.3µg/g, 61.2µg/g to 929.9µg/g, below detection limit to 4.2µg/g, 11µg/g to 27.µg/g, 4.2µg/g to 16.9µg/g, and below detection limit to 2.6µg/g, respectively. The most significant trace elements in the parent rocks are Cu, Pb, Zn and As. On average, the Cu, Pb and Zn concentrations are nearly identical in the altered andesite of 254.0µg/g, 236.9µg/g and 232.9µg/g, respectively. On the contrary, in volcanic breccia, Cu concentration is significantly lower, 42.1µg/g, than Pb, 535.3µg/g and Zn, 541.2µg/g, respectively.

Table 4. The concentration of trace elements in the hydrothermally altered andesite and volcanic breccia in Bukit Mantri gold mine área, Tawau, Sabah.

Id	Rock Type[alt.]	As	Ba	Cu	Pb	Zn	Cd	Cr	Ni	Ag
		µg/g								
JMG-01	And.[arg.]	25.4	102.7	131.2	430.1	548.7	0.2	15.5	6.5	<0.01
JMG-02	And.[arg.]	30.9	101.4	40.4	486.2	72	0.2	11.4	4.2	2.6
JMG-03	And.[arg.]	108.5	101	351.2	427	246.5	1.4	17.4	6.5	<0.01
JMG-04	And.[arg].	27.9	102.5	108.2	463.1	61.8	<0.01	25.4	4.2	<0.01
JMG-05	And.[prop.]	8.1	101	427.6	374.2	286.1	1.5	18.3	5.5	<0.01
JMG-06	And.[prop.]	11.6	101.2	22.9	237.6	929.9	4.2	27.8	14.1	<0.01
JMG-07	And.[arg.]	78.2	101.9	38.2	40.9	61.2	1.1	12.8	4.6	<0.01
JMG-08	And.[prop.]	13	103.8	33.7	31.9	67.4	<0.01	12.9	4.2	<0.01
JMG-09	And.[arg.]	32.7	102	221.5	491.9	82.1	0.4	20.8	4.4	<0.01
JMG-10	And.[si.]	54.3	101.4	1827.1	155.5	449.6	2.3	11	4.4	2.4
JMG-11	And.[arg.]	35.5	102.2	354.1	27.7	151.9	2.3	14.5	7.9	<0.01
JMG-12	Volc. Breccia	129.2	101.4	42.1	535.3	541.2	4.1	16.8	16.9	0.8
JMG-13	And.[prop.]	9	101.5	449.5	447.4	266.7	1.6	15.8	5.6	<0.01
JMG-14	And.[arg., sulph.]	15.8	101.1	21.2	117.7	233.6	0.8	11.3	4.8	<0.01
JMG-15	And.[arg., sulph.]	13.2	101.3	9.1	19.6	65.1	<0.01	12	4.5	<0.01
JMG-16	And.[arg., sulph.]	11.8	101.2	13	12.2	73.9	<0.01	12.4	5	<0.01
JMG-17	And.[arg., sulph.]	14	101.4	15.4	27.6	130.3	0.4	19.7	13.9	<0.01
Minimum		8.1	101	9.1	12.2	61.2	<0.01	11	4.2	<0.01
Maximum		129.2	103.8	1827.1	535.3	929.9	4.2	27.8	16.9	2.6
Average*, x̄		30.6	101.7	254.0	236.9	232.9	1.4	16.2	6.3	2.5

Remarks: Alt = alteration, And = andesite, arg. = argilised, prop. = propylitised, si. = silicified, sulp. = sulphidised, bdl = below detection limit, * = average exclude of volcanic breccia.

Cu, Pb and Zn have no variation with andesite alteration profiles, but As does, as it is relatively higher in argilised and silicified andesite and volcanic breccia than in propylitised andesite. Also, Zn appears to be sorbed onto secondary minerals (r=0.98, 0.86, and 0.88, with respect to SiO_2, Al_2O_3 and $Fe_2O_3^T$) (Table 5) than other trace elements, indicating its high susceptibility to sorption by secondary minerals. Ba, Cd, Cr, Ni and Ag made up the relatively less significant, and their concentrations are 101.0µg/g – 103.8µg/g, below the detection limit to 4.2µg/g, 11.0µg/g to 27.8µg/g, 4.2 µg/g to 16.9µg/g, and below the detection limit to 2.6µg/g, respectively. These suggest their concentration in parent rocks is lower and could have a minimum impact.

Table 5. The coefficient of correlations, r between SiO_2, $Fe_2O_3^T$, Al_2O_3 with trace elements in weathered andesite.

Item	As	Ba	Cu	Pb	Zn	Cd	Cr	Ni
SiO_2	0.43	0.04	-0.35	-0.44	-0.98	-0.03	0.22	-0.58
Al_2O_3	-0.16	-0.27	0.31	0.32	0.86	0.13	-0.47	0.38
$Fe_2O_3^T$	-0.47	0.28	0.03	0.52	0.88	-0.35	0.12	0.40

Remarks: calculated for samples JMG-01, JMG-04, JMG-07, JMG-08, JMG-11 and JMG-13, where secondary minerals appeared in XRD spectrograms.

CONCLUSION

Hydrothermal activities appear to influence the geochemical composition of parent rocks and the distribution and abundance of various minerals, such as pyrite and silicate minerals. Upon weathering, they both generate and consume acid. The significant concentration of sulphides, particularly associated with the widespread occurrence of pyrite, indicates a greater potential for acidity generation and, consequently, the release of numerous constituents, especially Cu, Pb, Zn and As, which have a substantially high concentration in the host rocks.

ACKNOWLEDGEMENT

I am thankful for the assistance provided by Mr Shamsul Arif Haruna, Mr Sze To Han Suon, Mr Edwin James and the rest of the technical team from Southsea Gold Sdn. Bhd. during the fieldwork. Special thanks are also extended to Mr Edwin James for his geologic field interpretation and optical micrographs of hydrothermally altered andesite thin sections specimens. Also, much appreciation is given to Dr Rashita binti Abd Rashid, Ms Norin Safrina binti Mustaffa Kamal, and Mr Sharizan bin Hashim on XRD and XRF analyses conducted at the Mineral Research Centre and Geochemical Laboratory Services of the Department of Mineral and Geoscience Malaysia.

REFERENCES

Clark, C. M., & Downs, R. T. (2004). Using the American Mineralogist Crystal Structure Database in the Classroom. *Journal of Geoscience Education, 52*(1), 76–80. https://doi.org/10.5408/1089-9995-52.1.76

Downs, R. T., & Hall-Wallace, M. (2003). Using the American Mineralogist Crystal Structure Database. *American Mineralogist*, *88*, 247–250. https://doi.org/10.5408/1089-9995-52.1.76

Haruna, S. A. (2016). *Geology and Mineral Exploration in the Bukit Mantri Gold Prospect, Wullersdorf Area, Tawau District*.

Mackenzie, W. S., Adams, A. E., & Brodie, K. H. (2017). Rocks and Minerals in Thin Section. In *Rocks and Minerals in Thin Section* (2nd Editio). CRC Press. https://doi.org/10.1201/9781315116365

Musta, B., Soehady, H. F. W., & Tahir, S. (2008). Geochemical characterization of volcanic soils from Tawau, Sabah. *Bulletin of the Geological Society of Malaysia*, *54*, 33–36. https://doi.org/10.7186/bgsm2008006

Nordstrom, D. K. (2011). Hydrogeochemical processes governing the origin, transport and fate of major and trace elements from mine wastes and mineralized rock to surface waters. *Applied Geochemistry*, *26*(11), 1777–1791. https://doi.org/10.1016/j.apgeochem.2011.06.002

Nordstrom, D. K., & Alpers, C. N. (1999). Geochemistry of acid mine waters. In G. S. Plumlee & M. J. Logsdon (Eds.), *The Environmental Geochemistry of Mineral Deposits, Part A. Processes, Techniques, and Health Issues: Society of Economic Geologist, Reviews in Economic Geology* (Vol. 6).

Plumlee, G. S. (1999). The Environmental Geology of Mineral Deposits. In G. S. Plumlee & M. J. Logsdon (Eds.), *The Environmental Geochemistry of Mineral Deposits, Part A. Processes, Techniques, and Health Issues: Society of Economic Geologist, Reviews in Economic Geology* (pp. 71–116).

Smith, K. S. (1999). Metal Sorption on Mineral Surfaces: An Overview with Examples Relating to Mineral Deposits. *Review in Economic Geology*, *6A-6B*, 161–182. https://doi.org/10.1.1.371.7008

Tahir, S., Musta, B., & Rahim, I. A. (2010). Geological heritage features of Tawau volcanic sequence, Sabah. *Bulletin of the Geological Society of Malaysia*, *56*(56), 79–85. https://doi.org/10.7186/bgsm2010012

Winter, J. D. (2014). *Principles of Igneous and Metamorphic Petrology* (Pearson Ne). Pearson Education Limited.

Yan, A. S. W. (1991). *Features of volcanic-hosted epithermal gold mineralization in the Nagos and Mantri areas, Sabah. Report No. SB 91/1*.

BorneoScience
The Journal of Science & Technology
Volume 44 Issue 1 : April 2023
Online ISSN : 2231-9085 | ISSN : 1394-4339

EFFECT OF ETHANOL TREATMENT ON SHRINKAGE OF OIL PALM TRUNK FOR THE DRYING PROCESS

Ahmad Fauzi Othman[1], Mohd Fadzil Arshad[2], Zakiah Ahmad[2], Amran Shafie[1], Junaiza Ahmad Zaki[1], Nur Hannani Abdul Latif[1], Mohd Azrul Naim[3*]

[1]Faculty of Applied Science, Universiti Teknologi Mara, Bandar Jengka, 26400 Bandar Tun Razak, Pahang
[2]College of Civil Engineering, Universiti Teknologi Mara, 40450 Shah Alam, Selangor
[3]Department of Biotechnology, Kulliyyah of Science, International Islamic University Malaysia, Jalan Sultan Haji Ahmad Shah, 25200, Kuantan, Pahang

Corresponding author: Mohd Azrul Naim, Email: aznaim@iium.edu.my

Received 25th Oktober 2022; Accepted 8th February 2023
Available online 20th April 2023
https://doi.org/10.51200/bsj.v44i1.4349

ABSTRACT. *Oil palm trunk is one of the promising biomass materials due to the high volume of unused waste components and increasing worldwide demand to replace conventional wood. This study investigated the feasibility of using ethanol as a drying agent for oil palm trunks with different dimensional surfaces (radial, tangential and longitudinal sections). The radial shrinkage percentage for the outer layer is 1.50% (untreated) and 1.22 % (treated). In comparison, the inner layer of the untreated sample was recorded at 2.54 % shrinkage and the treated sample was at 2.29%. The tangential sample for the inner untreated sample shows 2.60% and the treated sample shows 2.40%. The same pattern of shrinkage was shown for the tangential section on the outer layer as 1.81% and 1.10% of the untreated and treated sample respectively. For the longitudinal surface, the inner layer section of the untreated sample was recorded at 0.39% compared to the treated sample at 0.25%. In comparison, a longitudinal surface section for the outer layer of the untreated sample was recorded at 0.38%, while the treated sample was recorded at 0.33% shrinkage percentage. The effect of ethanol treatment on the shrinkage is significantly different between different sections (P-value: 0.01) and between the outer and inner layers (P-value: 0.02). The result suggested that ethanol treatment could be an option for the oil palm trunk drying process. Dried oil palm trunks can be utilized as a potential substitution for biomass and wood to produce various products.*

KEYWORDS. Oil palm trunk (OPT), shrinkage percentage, moisture content, ethanol

INTRODUCTION

The Malaysian wood industry is facing challenges in terms of sustaining the growth of the industry which is now critical due to a rapidly approaching shortage of raw materials (Ab Latib et al., 2022). Alternative sources have been sought after from sustainable biomass to replace natural timber fields. (Amira et al., 2020). Oil palm trunk is one such source that has been widely accepted as it is very

economical compared to solid wood. In addition, its performance is also comparable to solid wood in terms of stability and resistance to weather albeit with slight modification needed before its use (Hashim et al., 2012; Sulaiman et al., 2012).

Oil palm *(Elaeis guineensis)* of the palm family (*Arecaceae*) grows in the wildlands of West Africa and has been developed into an agricultural crop worldwide. The oil palm was introduced to Malaysia in early 1870 as an ornamental plant (Teoh, 2002). It then becomes the largest commercial plantation in Malaysia to date. As the largest commercial plantation, oil palm plantation creates huge quantities of oil palm trunks, oil palm shells, oil palm fronds, empty fruit brunch, and other related biomass (Kaniapan et al., 2021). Out of all oil palm-related biomass, the oil palm trunk is considered to be the highest value in terms of potential to be exploited (Abdul et al., 2012; Abdul Hamid et al., 2015; Eom et al., 2015).

Oil palm trunk has higher moisture content than other wood, ranging from 120% to over 500% (Lim & Gan, 2005; Wong et al., 2019). It is difficult to dry the moisture from oil palm trunk as it usually takes 7 to 12 days with a recovery rate of only 18.26% while the remaining lumber (81.70%) was considered a waste to dry via the industrial kiln dry process (Anis et al., 2016; Rais et al., 2021). The total drying time is an important parameter for oil palm trunks as it affects dimensioning, reduces degradation, prevents biological staining, and reduces transport costs (Murphy et al., 2021). On the other hand, reducing drying time will increase the defect on the wood surface such as cracking and twisting (Bakar et al., 1998).

The oil palm trunk drying method using ethanol has enormous potential as it has been used in many applications. For instance, ethanol also was used previously as a drying agent in medicinal plants (Silva et al., 2018), improving the pulping process from wood (Hochegger et al., 2019), and also for the precipitation of lignin (Hamzah et al., 2020). The advantages of ethanol are that it is a relatively cheap solvent, has complete miscibility with water, has a hardening effect, has a powerful dehydration capacity, and has a penetrability (Lai & Lü, 2012). Therefore, in this study, shrinkage of oil palm trunk using ethanol has been studied to explore the potential of ethanol as a treatment method for the drying process of the oil palm trunk.

MATERIALS AND METHODS

Oil palm trunk collection and preparation

A 25-year-old oil palm tree has been harvested from an oil palm plantation in UiTM Jengka, Pahang, Malaysia. Before the logging process, the tree height and diameter at breast height (DBH) were checked and recorded to ensure that the oil palm trunk was at a suitable size for the sampling (Migolet et al., 2020; Tan et al., 2014). A chainsaw (Husqvarna 372XP) was used in felling the oil palm tree. The top and the bottom part were removed, leaving approximately ~3 m of the oil palm trunk section, and subsequently, it was then cut into a disc shape. The disks were tagged with the outer and inner layer parts (Figure 1) by estimating 70% distance of the disc from the center of its inner layer while the remaining 30% was considered as the outer layer (Hashim et al., 2012). Disc shape oil palm trunk was then cut into cube sizes of 2 cm X 2 cm X 6 cm with sectional segregation of tangential, radial, and longitudinal parts. All samples were run in biological triplicates.

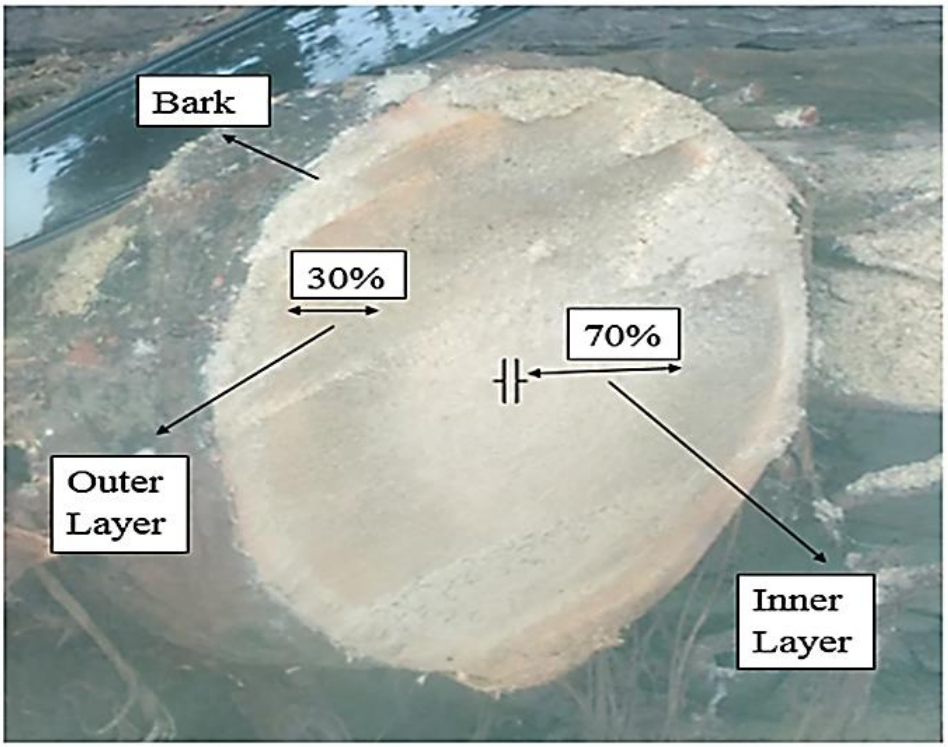

Figure 1. Disc cutting design of oil palm trunk. The inner layer was marked as 70% distance from its core and the remaining 30% distance was designated as an outer layer.

Ethanol-treated oil palm trunk samples

Oil palm trunk samples cut into cube sizes were then measured using a veneer caliper (Mitutoyo) before soaking with ethanol for calculation afterward. Ethanol (Supelco®) with 85% concentration was used for the soaking treatment process. Samples were soaked fully submerged in a closed container to prevent the early evaporation of ethanol for 24 hours (Figure 2). Next, the samples were dried using a drying oven (Memmert) with a constant temperature of 103±2 °C. The moisture content of each sample was determined by weighing the sample using an analytical balance (Shimadzu) before and after drying treatment until it came to a constant weight.

Figure 2. The soaking treatment process of cube-sized oil palm trunk (OPT) with ethanol. The samples were kept in a closed container at room temperature for 24 hours before drying.

Moisture and shrinkage calculation for the ethanol treatment process

Moisture Content (MC) from cube-sized oil palm trunk (OPT) soaked with ethanol was calculated following the equation as per British Standard Methods for testing small clear specimens of timber (BS373:1957).

$$\text{Moisture content (MC) \%} = \frac{air\ dried - oven\ dried}{oven\ dried} \times 100\%$$

Shrinkage of the cube-sized oil palm trunk (OPT) soaked with ethanol samples was also calculated following the equation as per British Standard Methods for testing small clear specimens of timber (BS373:1957) and the mean was recorded.

$$\text{Radial section shrinkage (\%)} = \frac{width\ green - width\ oven\ dry}{width\ green} \times 100\%$$

$$\text{Tangential section shrinkage (\%)} = \frac{width\ green - width\ oven\ dry}{width\ green} \times 100\%$$

$$\text{Longitudinal section shrinkage (\%)} = \frac{width\ green - width\ oven\ dry}{width\ green} \times 100\%$$

Statistical Analysis

Analysis of variance (ANOVA) of two factors without replication was carried out to assess statistical differences between radial, tangential, and longitudinal sections.

RESULTS AND DISCUSSION

The moisture content of different layers of oil palm trunk

Moisture content (median) of the prepared oil palm trunk (OPT) samples treated and untreated for both inner and outer layers is shown in Figure 3. The median moisture content of the untreated sample is 375% for the outer layer and 578% for the inner layer (Figure 3). The median moisture content for treated samples was 385% for the outer layer 585% for the inner layer and (Figure 3). Differences in moisture content between the inner layer and outer layer of oil palm trunk samples are due to the presence of parenchyma cells in the core layer higher compared to the outer layer. As a result, this affects the moisture content because parenchyma cell tends to absorb moisture (Mhd Ramle et al., 2012).

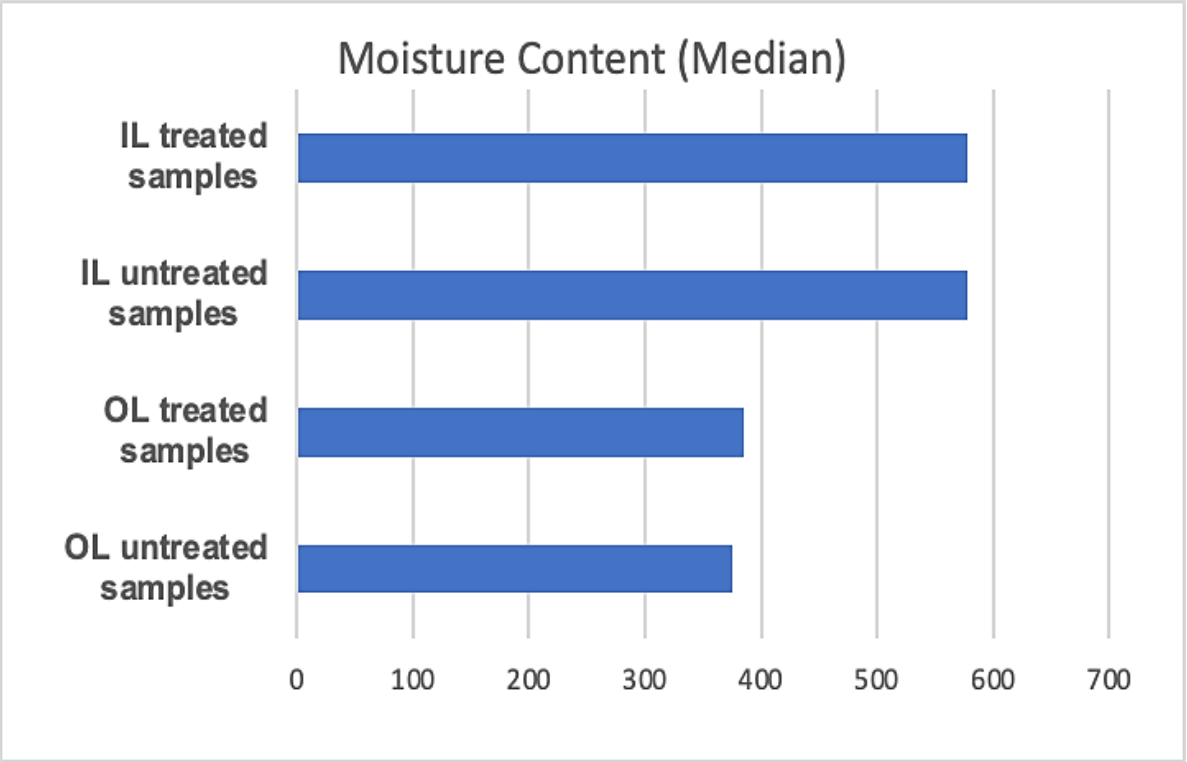

Figure 3. The median moisture content of untreated and treated samples of oil palm trunk (OPT) for both the inner layer (IL) and outer layer (OL).

Shrinkage of different sections of oil palm trunk

The radial layer section in the oil palm trunk is characterized by the vertical plane from the pith at the center of the tree heading out towards the bark, while the tangential section is made perpendicular to the rays and tangential to the annual rings and face of the oil palm trunk (Rosli et al., 2021)**.** On the other hand, the longitudinal section is a cut along the long axis of a structure.

Overall, the use of ethanol decreased the percentage of shrinkage significantly on radial, tangential and longitudinal surfaces (*p-value: 0.01*). On the radial surface section, the outer layer showed 1.50% shrinkage for an untreated sample and 1.22 % for the treated sample. In comparison, the inner layer of the untreated sample was recorded at 2.54 % shrinkage and the treated sample was at 2.29% (Table 1). The tangential sample for the inner untreated sample shows 2.60% and the treated sample shows 2.40% (Table 1). The same pattern of shrinkage was shown for the tangential section on the outer layer was 1.81% and 1.10% of untreated and treated samples respectively (Table 1). For the longitudinal surface, the inner layer section of the untreated sample was recorded at 0.38% compared to the treated sample at 0.33% (Table 1). In comparison, a longitudinal surface section for the outer layer of the untreated sample was recorded at 0.39% while the treated sample was recorded at 0.25% shrinkage percentage.

Table 1. Shrinkage percentage (mean) of a treated and untreated sample of radial, tangential and longitudinal layers.

	Radial		Tangential		Longitudinal	
	Untreated	Treated	Untreated	Treated	Untreated	Treated
Outer Layer	1.50	1.22	1.81	1.10	0.39	0.25
Inner Layer	2.54	2.29	2.60	2.40	0.38	0.33

From the data collected in this study, it is apparent that the shrinkage percentage of the inner layer of tangential, radial, and longitudinal sections is significantly higher compared to the outer layer (*P-value: 0.02*). The inner layer has parenchyma cells and more moisture than the outer layer and consequently could cause the sample to shrink faster compared to the outer layer (Mhd Ramle, 2021; Mhd Ramle et al., 2012). It has been presented that the feature of the vascular bundle is dense, fibrous, and at least hygroscopic while the parenchyma feature is soft, spongy, and highly hygroscopic (Abdul Hamid et al., 2015; Erwinsyah et al., 2007).

In this study, it was shown that ethanol could contribute significantly to the overall drying process of the oil palm trunk, especially for shrinkage. This improvement in drying properties was recorded despite the short time of exposure (24 hours), hence future studies should include different soaking times in ethanol. This was also the case for other plant-based materials such as coumarin leaves (Silva et al., 2018), pineapple (de Freitas et al., 2021), and melon (da Cunha et al., 2020). However, another important function of ethanol in the drying process is to improve attributes of the dried material such as rehydration capacity and shrinkage (Funebo et al., 2002), color (Pang, 2006) aroma retention (Corrêa et al., 2012) and vitamin C retention ((Santos & Silva, 2009). In general, ethanol made the sample stable quickly and prevented the sample from overdrying and damaging its physical properties (de Freitas et al., 2021; Funebo et al., 2002). This improvement of plant material by ethanol is an attractive prospect for the oil palm trunk drying process in which the material is being protected before conversion to end-products such as chipboard, composite panels, and plywood.

CONCLUSION

In this study, it can be concluded that between three-surface directions (tangential, radial, and longitudinal), the tangential section has the most shrinkage, followed by radial and longitudinal. It is also clear in this study that the inner layer of the oil palm trunk is easily shrunk after ethanol treatment in comparison to the outer layer. This is due to the presence of parenchyma cells in a core layer that easily absorbs and releases water in comparison to the presence of a vascular bundle in the outer layer that reduces the rate of shrinkage. The shrinkage between untreated and treated samples shows that the treated sample has higher shrinkage percentage compared to the untreated sample (*P-value: 0.01*). The shrinkage percentage of the inner layer of tangential, radial, and longitudinal sections is significantly higher compared to the outer layer (*P-value: 0.02*). The shrinkage was recorded despite the short exposure of samples to ethanol (24 hours) and related to the drying time. However, another important property of ethanol is to prevent over-drying of the oil palm trunk. From this study, it can be summarised that ethanol could be the solution for dimensional stability of oil palm drying.

ACKNOWLEDGEMENT

This study was funded by "Dana Dalam Negeri (DDN) Lestari Khas Fasa 2 with Grant Number: 600-TNCPI 5/3/DDN(06)(009/2021).

REFERENCES

Ab Latib, H., Ratnasingam, J., Mariapan, M., Othman, K., Amir, M., Choon Liat, L., Lee, Y. Y., Ioras, F., Farrokhpayam, S. R., & Jegatheswaran, N. (2022). Malaysian Timber Industry Policy: Achievements, Challenges, and Lessons Learned. *BioResources*, *17*(1), 299–315.

Abdul, H. P. S., Jawaid, M., Hassan, A., Paridah, M. T., & Zaido, A. (2012). Oil Palm Biomass Fibres and Recent Advancement in Oil Palm Biomass Fibres Based Hybrid Biocomposites. *Composites and Their Applications*, *August*. https://doi.org/10.5772/48235

Abdul Hamid, Z. A., Arai, T., Sitti Fatimah, M. R., Kosugi, A., Sulaiman, O., Hashim, R., Nirasawa, S., Ryohei, T., Lokesh, B. E., Sudesh, K., Murata, Y., Saito, M., & Mori, Y. (2015). Analysis of Free Sugar and Starch in Oil Palm Trunks (Elaeis Guineensis Jacq.) from Various Cultivars as a Feedstock for Bioethanol Production . *International Journal of Green Energy*, 150218144136008. https://doi.org/10.1080/15435075.2014.910786

Amira, N., Armir, Z., Zakaria, S., Begum, R. A., Chamhuri, N., Ariff, N. M., Harun, J., Laila, N., Talib, M., & Kadir, M. A. (2020). Malaysia wood industries. *BioResources*, *15*(2), 2971–2993.

Anis, M., Noor, A. S., Ismail, S., Halimah, M., & Astimar, A. A. (2016). Recovery of oil palm lumber. *Journal Palm Oil Developments*, *64*, 7–10.

Corrêa, J. L. G., Braga, A. M. P., Hochheim, M., & Silva, M. A. (2012). The Influence of Ethanol on the Convective Drying of Unripe, Ripe, and Overripe Bananas. *Drying Technology*, *30*(8), 817–826. https://doi.org/10.1080/07373937.2012.667469

da Cunha, R. M. C., Brandão, S. C. R., de Medeiros, R. A. B., da Silva Júnior, E. V., Fernandes da Silva, J. H., & Azoubel, P. M. (2020). Effect of ethanol pretreatment on melon convective drying. *Food Chemistry*, *333*, 127502. https://doi.org/https://doi.org/10.1016/j.foodchem.2020.127502

de Freitas, L. D. C., Brandão, S. C. R., Fernandes da Silva, J. H., Sá da Rocha, O. R., & Azoubel, P. M. (2021). Effect of Ethanol and Ultrasound Pretreatments on Pineapple Convective Drying. *Food Technology and Biotechnology*, *59*(2), 209–215. https://doi.org/10.17113/ftb.59.02.21.7045

Eom, I. Y., Yu, J. H., Jung, C. D., & Hong, K. S. (2015). Efficient ethanol production from dried oil palm trunk treated by hydrothermolysis and subsequent enzymatic hydrolysis. *Biotechnology for Biofuels*, *8*(1). https://doi.org/10.1186/s13068-015-0263-6

Erwinsyah, Bues, C. T., & Richter, C. (2007). Thermal Insulation Material Made from OPEFB Fibres.pdf. *Biotropia*, *14*(1), 32–50. chrome-extension://oemmndcbldboiebfnladdacbdfmadadm/https://journal.biotrop.org/index.php/biotropia/article/download/23/451

Funebo, T., Ahrné, L., Prothon, F., Kidman, S., Langton, M., & Skjöldebrand, C. (2002). Microwave and convective dehydration of ethanol treated and frozen apple – physical properties and drying kinetics. *International Journal of Food Science \& Technology*, *37*(6), 603–614. https://doi.org/https://doi.org/10.1046/j.1365-2621.2002.00592.x

Hamzah, M. H., Bowra, S., & Cox, P. (2020). Effects of Ethanol Concentration on Organosolv Lignin Precipitation and Aggregation from Miscanthus x giganteus. *Processes*, *8*(7). https://doi.org/10.3390/pr8070845

Hashim, R., Aidawati, W. N., Nadhari, W., Sulaiman, O., Sato, M., Hiziroglu, S., Kawamura, F., Sugimoto, T., Guan, T., & Tanaka, R. (2012). Palm binderless particleboard. In *BioResources* (Vol. 7, Issue 1).

Hochegger, M., Cottyn-Boitte, B., Cézard, L., Schober, S., & Mittelbach, M. (2019). Influence of Ethanol Organosolv Pulping Conditions on Physicochemical Lignin Properties of European Larch. *International Journal of Chemical Engineering*, *2019*. https://doi.org/10.1155/2019/1734507

Kaniapan, S., Hassan, S., Ya, H., Nesan, K. P., & Azeem, M. (2021). The utilisation of palm oil and oil palm residues and the related challenges as a sustainable alternative in biofuel, bioenergy, and transportation sector: A review. *Sustainability (Switzerland)*, *13*(6). https://doi.org/10.3390/su13063110

Lai, M., & Lü, B. (2012). *3.04 - Tissue Preparation for Microscopy and Histology* (J. B. T.-C. S. and S. P. Pawliszyn (Ed.); pp. 53–93). Academic Press. https://doi.org/https://doi.org/10.1016/B978-0-12-381373-2.00070-3

Lim, S., & Gan, K. (2005). Characteristics and utilisation of oil palm stem. *Timber Technology Bulletin*, *35*, 1–12.

Mhd Ramle, S. F. (2021). Chemical Composition of Parenchyma and Vascular Bundle from Elaeis guineensis. In H. Kamyab (Ed.), *Elaeis guineensis* (p. 13). IntechOpen. https://doi.org/10.5772/intechopen.98421

Mhd Ramle, S. F., Sulaiman, O., Hashim, R., Arai, T., Kosugi, A., Abe, H., Murata, Y., & Mori, Y. (2012). Characterization of Parenchyma and Vascular Bundle of Oil Palm Trunk as Function of Storage Time. *Lignocellulose*, *1*(1), 33–44.

Migolet, P., Goïta, K., Ngomanda, A., & Biyogo, A. P. M. (2020). Estimation of aboveground oil palm biomass in a mature plantation in the Congo Basin. *Forests*, *11*(5), 1–23.

https://doi.org/10.3390/F11050544

Murphy, D. J., Goggin, K., & Paterson, R. R. M. (2021). Oil palm in the 2020s and beyond: challenges and solutions. *CABI Agriculture and Bioscience*, *2*(1), 1–22. https://doi.org/10.1186/s43170-021-00058-3

Pang, S. (2006). *Using methanol and ethanol vapours as drying media for producing bright colour wood in drying of radiata pine*.

Rais, M. R., Bakar, E. S., Ahaari, Z., Lee, S. H., Soltani, M., Ramli, F., & Bawon, P. (2021). Drying performance, as well as physical and flexural properties of oil palm wood dried via the super-fast drying method. *BioResources*, *16*(1), 1674–1685. https://bioresources.cnr.ncsu.edu/resources/drying-performance-as-well-as-physical-and-flexural-properties-of-oil-palm-wood-dried-via-the-super-fast-drying-method/

Rosli, R. A., Harumain, Z. A. S., Zulkalam, M. F., Hamid, A. A. A., Sharif, M. F., Mohamad, M. A. N., Noh, A. L., & Shahari, R. (2021). Phytoremediation of Arsenic in Mine Wastes by Acacia mangium. *Remediation Journal*, *31*(3), 49–59.

Santos, P. H. S., & Silva, M. A. (2009). Kinetics of L-Ascorbic Acid Degradation in Pineapple Drying under Ethanolic Atmosphere. *Drying Technology*, *27*(9), 947–954. https://doi.org/10.1080/07373930902901950

Silva, M. G., Celeghini, R. M. S., & Silva, M. A. (2018). Effect of ethanol on the drying characteristics and on the coumarin yield of dried guaco leaves (Mikania laevigata schultz BIP. Ex Baker). *Brazilian Journal of Chemical Engineering*, *35*(3), 1095–1104. https://doi.org/10.1590/0104-6632.20180353s20160481

Sulaiman, O., Salim, N., Nordin, N. A., Hashim, R., Ibrahim, M., & Sato, M. (2012). The potential of oil palm trunk biomass as an alternative source for compressed wood. *BioResources*, *7*(2), 2688–2706. https://doi.org/10.15376/biores.7.2.2688-2706

Tan, K. P., Kanniah, K. D., & Cracknell, A. P. (2014). On the upstream inputs into the MODIS primary productivity products using biometric data from oil palm plantations. *International Journal of Remote Sensing*, *35*(6), 2212246.https://doi.org/10.1080/01431161.2014.889865

Teoh, C. H. (2002). The palm oil industry in Malaysia: From seed to frying pan. In *WWF* (Issue November).http://www.senternovem.nl/mmfiles/WWF_palm_oil_industry_Malaysia_tcm24-195179.pdf

Wong, T., Lim, S., Gan, K., & Chung, R. (Eds.). (2019). *A Dictionary of Malaysian Timbers: 3rd Edition* (3rd Editio). Forest Research Institute Malaysia.

BorneoScience
The Journal of Science & Technology
Volume 44 Issue 1 : April 2023
Online ISSN : 2231-9085 | ISSN : 1394-4339

POZZOLAN EFFECT ON THE MECHANICAL PROPERTIES OF SCBA BLENDED CEMENT TREATED SOIL

Roziah K[1], Kok Shien N[1], Farzana M.A[1], Siti Fatimah S[1], Azura A[1]

[1]Civil Engineering Studies, College of Engineering, Universiti Teknologi MARA, Cawangan Pulau Pinang, 13500 Permatang Pauh, Pulau Pinang, Malaysia

Received 26th October 2022; Accepted 8th February 2023
Available online 20th April 2023
Doi : https://doi.org/10.51200/bsj.v44i1.4355

ABSTRACT. *The recent agricultural and industrial waste reduction research has focused on monetary, sustainable environment, and technological considerations. Discarded raw materials such as rice husk ash, fly ash, coir fiber and silica fumes were widely explored and successfully utilized as blending elements for cement. Current studies have proved that Sugarcane Bagasse Ash (SCBA) produced from sugar production has a pozzolanic reaction due to the high substance of amorphous silica in this raw material. This research would boost the insight of potential blending agents that can reduce the cost and stabilize problematic soil. This study intends to evaluate the effect of SCBA blended cement on improved soil's mechanical properties, including the shear strength and the compressibility of the treated soil. Unconfined Compressive Strength test was conducted to attain the compressive behavior, while the One-Dimensional test was performed to examine the compressibility behavior. The tested samples with SCBA show a beneficial effect in terms of both compressive strength and compressibility. This study proved that SCBA could be applied at least as a partial substitute to the Portland cement.*

KEYWORDS. Sugarcane bagasse ash, pozzolanic reaction, compressive strength, compressibility

INTRODUCTION

Soft soil is usually categorized as soil with poor shear strength and highly compressible and low permeability [1]. Generally, construction challenges in this type of soil are unsatisfactory bearing capacity, extreme post-construction settlement and uncertainty in excavation and embankment construction [2,3]. To enhance the strength and engineering properties of the problematic soil, numerous stabilization techniques with the addition of materials such as sugarcane bagasse ash [4,5], rice husk ash [6,7], cement [8,9], fly ash [10,11], and other additives [12,13] are often used.

Lime and cement are the most common stabilizers used to improve soil properties. However, these manufactured stabilizers are cost-consuming and not environmentally friendly. WBCSD [14] reported cement contributed roughly 5%-8% of global Carbon Dioxide production and is projected to rise to 1.2% every year till it reaches 4.4 billion tons around 2050.

With the escalating request from the whole world for more sugar and ethanol-producing in recent eras, undesirable waste has significantly risen. However, the waste can be used as fuel to stoke boilers that generate steam for electricity production. This incinerating process's finishing product is sugarcane bagasse ash (SCBA). Bagasse is a discarded product from sugar factories after the process of extraction of liquid from sugarcane. SCBA is a pozzolan material that contains a high amount of siliceous and aluminous material [15]. According to Frías *et al*. [15] pozzolan may possess a bit or no cementitious amount. But with the existence of water, it will react chemically along with calcium hydroxide at a typical temperature to produce composites having cementitious properties.

Besides that, the previous research demonstrated the silica content amount in the SCBA is higher than in other additives [16,17]. Therefore, the SCBA has a vast potential alternative to be used as a partial cement substitute compared to other waste materials. Numerous types of research have been performed by using SCBA as partial or total substitution of Portland cement as inert material in compacted soil blocks [18], road constructions [19], soft soil improvement [20,21] and others [22,23].

Abbasi and Zargar [24] reported that workability, mechanical strength, and concrete durability are improved by replacing cement with SCBA. According to Kantinaris [25] SCBA can be used in commercial cement and composite manufacturing. Saini *et al.* [26] and Kharade *et al*. [27] investigated the utilization of SCBA in stabilizing expansive soil. Their studies indicated that the compressive strength of soft soil improves slowly with the rise of the percentage of SCBA up to 5% and 6% without any extra chemical or cementing substance. However, an additional percentage of SCBA can initiate a decrease in UCS value. These actions are credited to the accessibility of an unsatisfactory volume of water necessary for pozzolanic reactions at elevated bagasse ash quantities.

One of the essential relationships observed in the soil stabilization of problematic soil samples is the variation of Maximum Dry Density and Optimum Moisture Content. In addition, stabilized peat by the utilization of SCBA to substitute cement in this soil has been investigated by several researchers. The findings indicated that the mechanical properties in the modification improved peat by applying SCBA were noticeably increased [27].

An increase in Optimum Moisture Content (OMC) and a decrease in Maximum Dry Density (MDD) values have been reported by [21,28,29] when SBCA was used as an additive. The rise in OMC was ascribed to the addition of water content during the hydration process, while the decrease in MDD value was credited to the lightweight SCBA in contrast with the soft soil used. The statement demonstrates that SCBA can be utilized as a soil enhancement means to reduce the settlement behaviour of strengthened soil.

Abu Talib *et al*. [3] and Kamaruidzaman *et al*. [20] reported in their study regarding a substantial lessening of the void ratio for ideal peat-cement-SCBA mixtures as contrasted to natural peat. The finding shows that the stabilized peat of secondary compression index/ compression index ratios (Cα/Cc) declined radically compared to untreated peat. This condition indicated that the stabilized soil mixture effectively decreased the secondary compression.

This article represents the findings of a thorough study on the mechanical properties of stabilized local soft soil in Pulau Pinang featuring Sugarcane Bagasse Ash (SCBA) and cement, which include the shear strength properties and the compressibility of the treated soil. The Unconfined

compressive Strength Test was performed to attain the compressive behaviour, while the One-Dimensional Test examined the compressibility behaviour. The subsequent sections represent the experimental process, the findings of numerous tests performed on stabilized modification soils and finally followed by the conclusions.

METHODOLOGY

The problematic soil utilized in this experiment was obtained from the construction site located at Bukit Tengah, Pulau Pinang. The disturbed soil sample was collected at a depth of 2.0 m to avoid the inclusion of organic material. The soil is greyish-black in colour. The Cone Penetrometer Test was performed to classify the soils by following the British Standard 1337 Part 2.

Table 1 shows the physical properties of natural soil. The natural soil was classified as SILT of Intermediate Plasticity (MI) according to the USCS classification system. The natural Moisture Content and Dry Densities were 24% and 1.553 g/cm^3, correspondingly. A Standard Proctor Test was performed on untreated soil to obtain the compaction characteristics of MDD and OMC. The test was performed according to British Standard 1337 Part 4. The Unconfined Compressive Strength (UCS) value obtained from the soil was 18.7 kN/m^2, categorized as very soft and problematic soil.

Table 1. Physical and mechanical properties of natural soil

Soil Characteristic	Value & Description
Moisture Content, MC (%)	24
Percentage of fines soil (%)	1.5
Optimum Moisture Content, OMC (%)	48.5
Maximum Dry Density, MDD (g/cm^3)	1.553
Unconfined Compressive Strength, UCS (kN/m^2)	18.7
Specific Gravity (G_s)	2.55
Liquid Limit, w_L (%)	42.24
Plastic Limit, w_P (%)	26.63
Plasticity Index, I_P (%)	15.61
Soil Classification	SILT of Intermediate Plasticity (MI)

The sugarcane's scientific name is "Saccharum Officinarum" which is typically used for making raw sugar. Figure 1 shows the location of the sugar cane fields. The efficacy of a pozzolan is primarily associated with its silica substance and the crystallinity of silica. Amorphous or partially crystalline silica is essential for developing pozzolanic reactions together with calcium hydroxide.

The burning requirements, such as the optimum temperature and the appropriate burning time, were monitored to produce high-quality SCBA. Besides that, a proper kiln or furnace was used to burn sugarcane bagasse. According to the earlier research, burning the bagasse in a furnace with a high-level temperature between 500 °C to 800 °C will generate good quality amorphous silica. However, the crystallinity in SCBA after the temperature of burning activities greater than 800 °C will produce

poorer pozzolanic properties [30,31]. In this research, the baggage ash was obtained from burning sugarcane baggage in a furnace of 800ºC.

Particle breaking of SCBA is an essential procedure to monitor the particle size of the material as it will modify the crystalline compounds and pozzolanic activities. The most appropriate size of SCBA to be adopted in this study is equivalent to the size of cement used, which is 2µm. The percentage SCBA used is 3%, 6%, and 9% for each blended sample. These percentages of SCBA are selected based on previous studies [5,27].

Figure 1. The location of the sugarcane fields

OPC Type I has been used in this research because it was suitable for various general purposes in construction and had an outstanding binding property that provides better strength to any structural or infrastructural components. Table 2 represents the chemical properties of soil, OPC, and SCBA. The higher value of silica and oxygen elements in SCBA shows good potential to serve as good pozzolanic material. Two samples of untreated soil and cement-treated soil mixed with SCBA were tested for three main properties: physical, mechanical, and chemical. The percentages of cement used were 3%, 5%, and 10%.

Table 2. Chemical properties of soil, OPC and SCBA

Element	Soil (%)	OPC (%)	SCBA (%)
Carbon, C	21.181	6.851	5.496
Oxygen, O	52.783	41.018	38.029
Magnesium, Mg	0.352	0.451	0.451
Aluminum, Al	8.251	1.077	0.358
Silica, Si	13.235	5.459	11.567
Iron, Fe	2.100	1.371	0.520

A sequence of laboratory experiments was performed on untreated and treated soil to accomplish this study's objectives, including the Unconfined Compressive Test (UCT) and One-Dimensional Consolidation (Oedometer) test. The tests had been conducted for soils with and without SCBA. To prepare the remolded sample, the soil was weighed and added with specific percentages of cement (3%, 5%, and 10%) and SCBA (3%, 6%, and 9 %) inside the plastic bag in the dry form.

For the UCT test, the sample was tested on three curing days: days 0, 3, and 7. Later, water was combined into the mixture and was carefully mixed until a consistent color was observed. The water added refers to the value of natural moisture content. Table 3 demonstrates the design mix of the samples to be tested on the mechanical properties and chemical properties.

Table 3. Design mix of the samples

Curing Day	OPC (%)	SCBA (%)
0	3	0
3		3
7		6
		9
0	5	0
3		3
7		6
		9
0	10	0
3		3
7		6
		9

The sample's design mix is prepared using data in Table 3. The blended soil samples were compressed in a cylindrical mold with a diameter of 38 mm and a height of 76 mm until the desired density and moisture content of 1.553 g/cm^3 and 24% were achieved. Then the compacted soil was extruded, wrapped with clear plastic, and stored in a desiccator for curing processes. After that, the UCS tests were performed in the laboratory as per British Standard 1337 Part 7 on each sample to obtain the strength for different percentages of cement, SCBA, and curing period, respectively.

The estimation of the rate amount of consolidation settlements is crucial for any structure built on a compressible soil layer. Hence, the One-Dimensional Consolidation test (according to British Standard 1377 Part 5) was conducted to determine the effect of SCBA (3%, 6%, 9%, and 12%) based on the dry density of soil as an additive on the consolidation settlement parameter of cement-treated soil. This study tested soil samples with 3%, 5% and 10% cement.

The ash-cement-soil mixture was compacted in a cylindrical mold until the required density of 1.553 g/cm^3 was attained. Then, the ring with a diameter of 50 mm and a height of 20 mm was pressed into the soil. The top and bottom of the ring were trimmed using a palette knife so that the ring's top and bottom were clean. The soil samples were submerged in the water for 24 hours before the test was conducted.

RESULT AND DISCUSSION

Effect of SCBA on UCS

The UCT tests were conducted 2 hours after the sample was prepared. The experimental results of the strength of the treated soils with different proportions of cement (3%, 5%, and 10%) and SCBA are shown in graphs Figure 2 to Figure 4. Based on the findings, the shear strength of the treated soil improved as the percentages of SCBA increased.

The SCBA contains a high-level quantity of silica and acts as a fine pozzolan. This indicates that adding SCBA can enhance the compressive strength of the soil samples. It can hydrate when there is liquid and react with the remaining calcium hydroxide of cement to produce pozzolanic compounds, hence further enhancing the soil strength [32]. The result justifies that the SCBA containing a high amount of silica is suitable for blending components for cement.

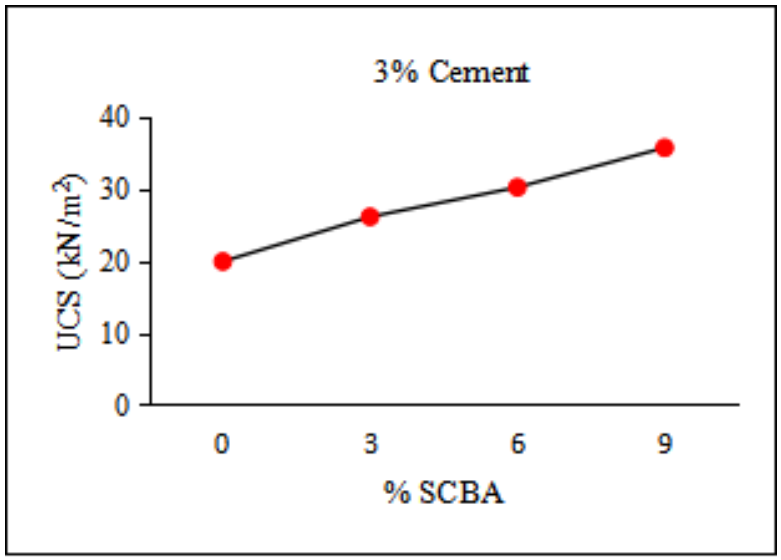

Figure 2. Effect of SCBA on UCS (3% Cement)

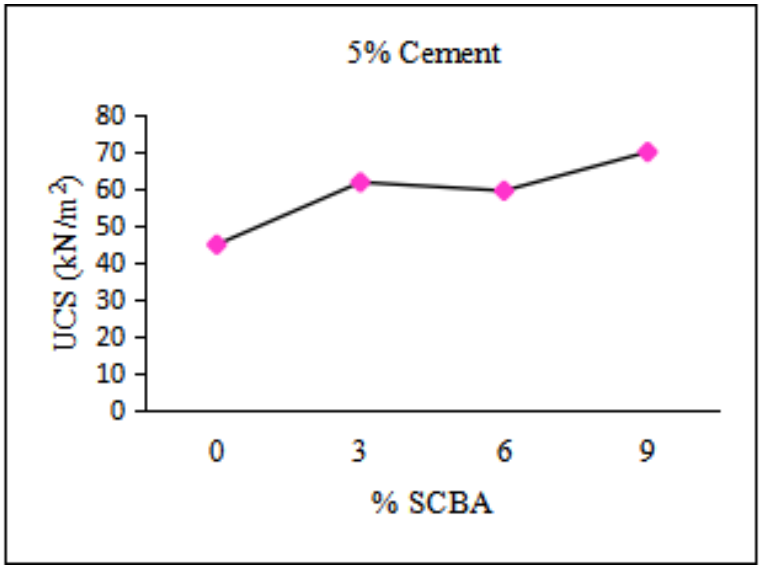

Figure 3. Effect of SCBA on UCS (5% Cement)

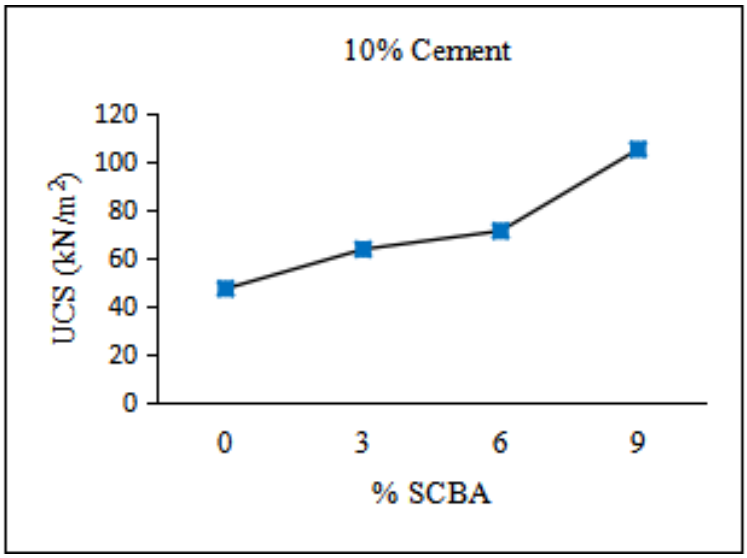

Figure 4. Effect of SCBA on UCS (10% Cement)

For each percentage of cement, the samples with the highest UCS values were those with the addition of 9% SCBA. This finding is supported by a previous study that the UCS value of the treated soil is more significant when the percentage of the ash is higher but up to optimal limit replacement for SCBA [29,33]. The results of a 5% cement mix with 9% SCBA are higher than 10% cement alone, indicating that the SCBA can be employed as a partial substitution for cement. However, in this study, the optimum limit of the SCBA is unknown.

Effect of Cement on UCS

The successful soil stabilization using pozzolanic material is only accomplished by mixing the waste material with the Portland cement. The OPC will activate the chemical reaction with the help of water. Then, the blended material becomes hardened and durable as the cement hydrates and strengthens. Figure 5 shows the effect of cement on Unconfined Compressive Strength.

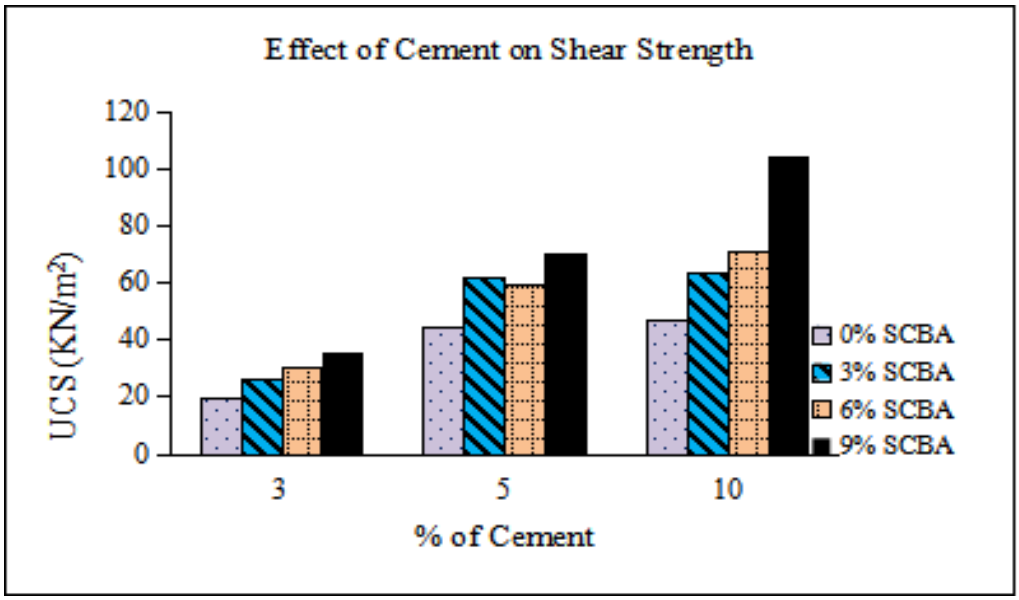

Figure 5. Effect of cement on UCS

In this experiment, the cement utilized as an additional additive with SCBA to enhance the soil properties were 3%, 5%, and 10%. The graph shows, once 3% of the cement added to the mix of different percentages of SCBA (0%, 3%, 6%, and 9%), the strength improved to 7%, 40.3%, 62.4%, and 91.9% respectively. The test then proceeds to the new samples with the addition of 5% of cement. The result indicates that the strength value of stabilized soil increased to 140.3%, 231.25%, 218.82%, and 275.3%, correspondingly. These strength increments were demonstrated to be three times greater than untreated soil.

When a similar test is repeated to 10% of cement, the strength of treated soil increases tremendously by 153%, 240.9%, 281.7%, and 464%, correspondingly. The result demonstrates that when the percentage of cement increases, the compressive strength increases likewise. The outcomes indicate the amount of cement added influences the soil strength. The more adhesive added, the higher strength of the mixture.

The result above was in line with Xiao & Lee [8] study where when the cement, additive, water, and soil combine, primary hydration will occur. Then, the secondary pozzolanic reaction will take over when the pore chemistry in the soil structure attains an alkaline form. This process is due to early strength improvement due to developing earlier cementitious products and drying up the soil-cement mix.

Effect of Curing Time on UCS

Unconfined Compressive Strength (UCS) values blended Cement-SCBA-Soil sample for 3% SCBA and different percentages of cement (3%, 5%, and 10%) were evaluated by examining the effect of curing time as illustrated in Figure 6. The blended Cement-SCBA-Soil sample was cured for 3 and 7 days. The curing sample was compared with an immediately blended soil sample from 0-Day curing time to see the results of the curing period on the soil samples. The UCS values for 0-Day curing were 26.1, 61.6, and 63.4 kN/m^2. When the sample was cured for 3-Days, the UCS increased to 52.8, 66.3, and 89 kN/m^2. Later, when the samples were cured for 7-Days, the UCS value also rose to 70.3, 83.3, and 161.9 kN/m^2 correspondingly. This situation signifies the effect of continuing the hydration process over time.

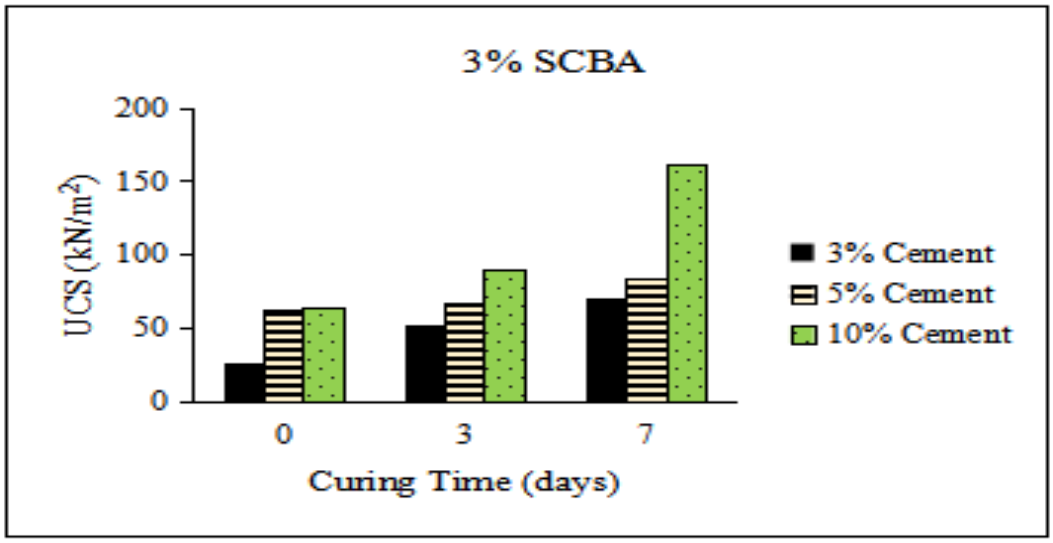

Figure 6. Effect of Curing on UCS of 3% SCBA

Figures 7 and 8 show the effect of curing time on UCS blended Cement-SCBA-Soil samples for 6% and 9% of SCBA and different percentages of cement (3%, 5%, and 10%). Similar to the previous SCBA 3% sample result, the UCS values significantly improved when the curing time was extended from 3 to 7 days. The result demonstrates drastic escalations of the UCS amount for cement by 10% with 7-Days curing. Testing results indicated that the additions of 3 and 7 days of curing time for the cement-SCBA-soil sample improved the structure of the admixtures leading to an elevated amount of strength compared to 0-Day curing.

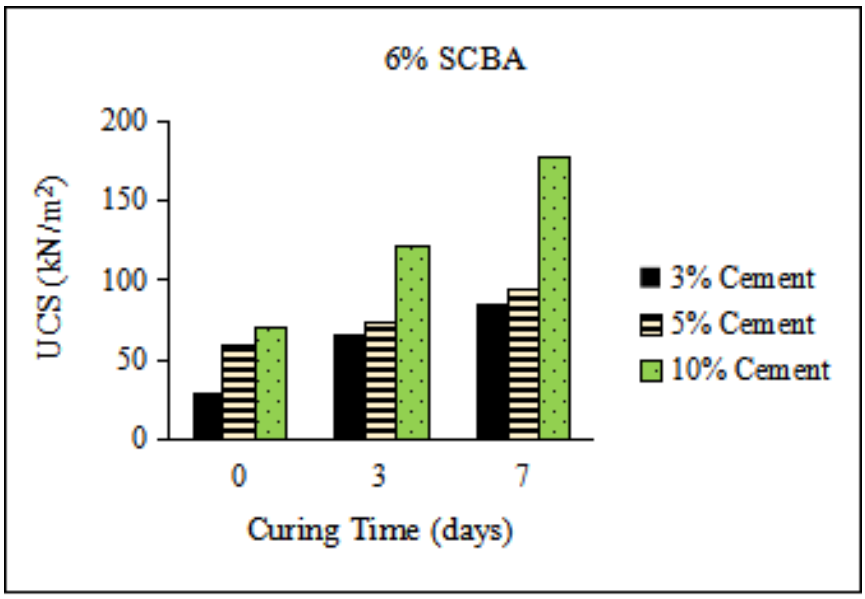

Figure 7. Effect of Curing on UCS of 6% SCBA

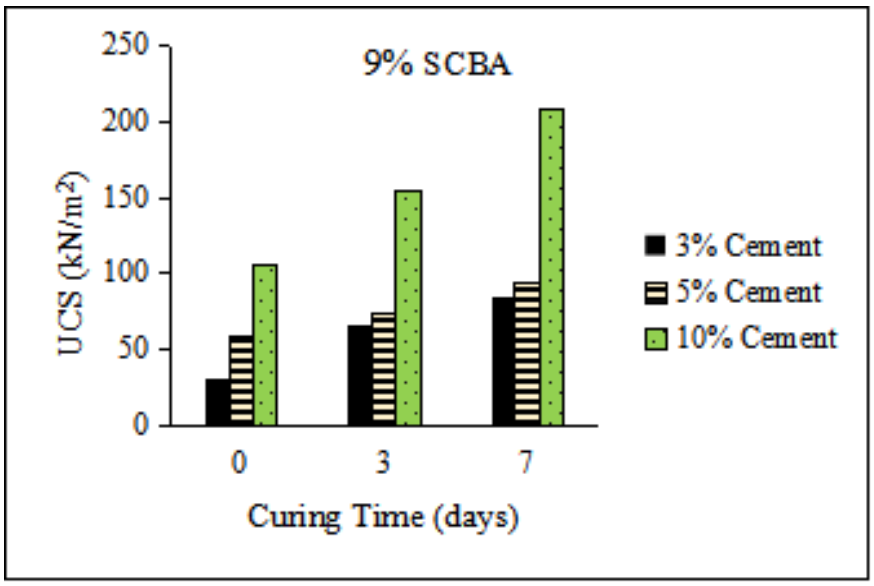

Figure 8. Effect of Curing on UCS of 9% SCBA

For the sample with the lowest percent of OPC and SCBA, the strength increases from 19.9 kN/m^2 on Day 0 to 52.4 kN/m^2 on Day 7. The increase of the UCS is about 1.6 times from Day 0 to Day 7. Comparable to samples with the highest percent of OPC and SCBA, the strength improves drastically

from 104.9 kN/m^2 on Day 0 to 208.9 kN/m^2 on Day 7. The result shows an increment of about 100% before curing and after 7-Days of curing. The hydration and pozzolanic processes of soil, cement, and SCBA occur from time to time. The enhancement of strength increases as the hydration and cementation reaction increases with the curing time [34,35].

The result illustrates the strength of the soil improved as the curing period increased due to the reaction between soil, cement, and SCBA. The pozzolanic behaviour was maximized between 3 and 7 days of curing. This condition explains by Abu Talib *et al*. [3] that the extreme escalation in the UCS earlier seven days of curing was primarily anticipated to the hydration reaction of the cement, the mixture of the filling effect of both silica plus SCBA, and as well as pozzolanic reaction.

Effect of SCBA on Consolidation Characteristic

Typically, soil subjected to vertical stresses will cause volume change through the rearrangement of soil grains. The total volume change is associated with the difference in the quantity of water in the soil. Water dissipated from the soil voids contributes to the deformation or settlement. This process takes time and varies with the permeability of the soil. The permeability is affected by particle distribution of the soil as the finer the soil particle, the lower the permeability [36].

The One-Dimensional Consolidation test was performed to obtain the consolidation characteristics of the soil. Figure 9 and Figure 10 present the relationship between stress (σ) applied and the coefficient of volume compressibility (mv) of 3% and 5% of OPC, respectively. The results depicted that the untreated soil has the highest volume of compressibility compared to the treated soil. The cement-treated soil with SCBA shows significant improvement in reducing the compressibility of the soil. The existence of OPC and SCBA has proven to uphold the soil particles simultaneously and strengthen the saturated soil.

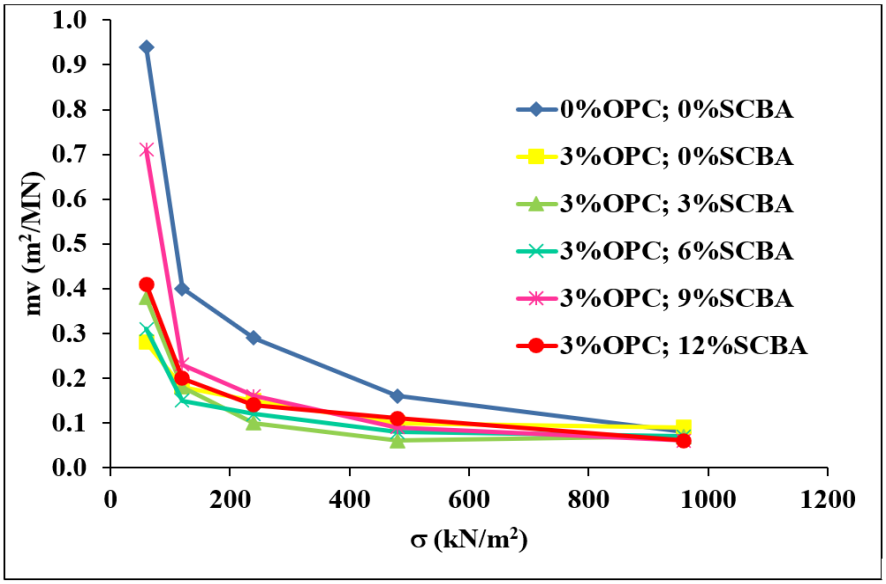

Figure 9. Change of m_v with stress for 3% OPC

The One- The test findings reveal that the soils with 3% SCBA for 3% and 5% OPC had the lowest volume of compressibility at the early loading stages. Meanwhile, at the subsequent loading stage, soil with 12% of SCBA has the lowest volume of compressibility for both 3% and 5% OPC. However, this is not obvious as other SCBA contents have a relatively small difference in the m_v value.

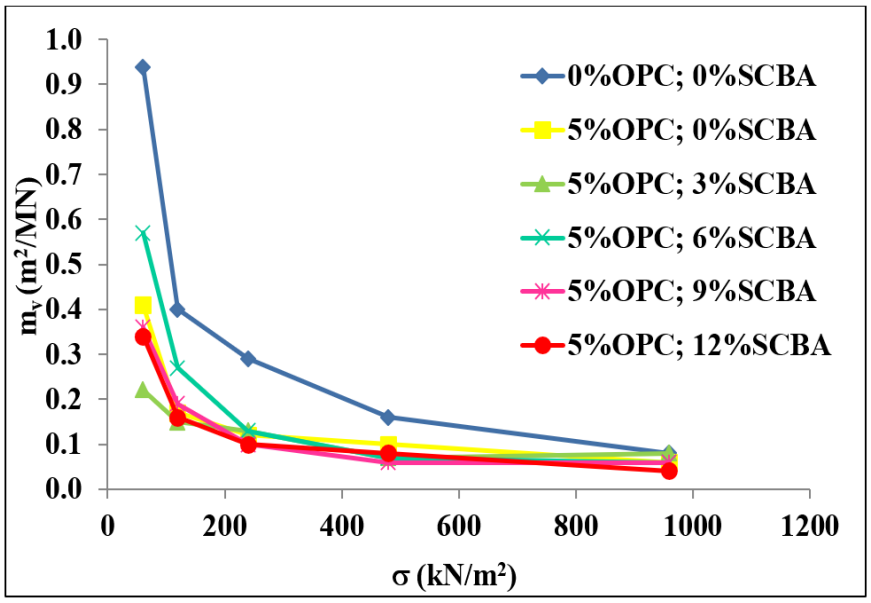

Figure 10. Change of m_v with stress for 5% OPC

In summary, the improvement of the soil strength is attributed to the inclusion of fine particles of SCBA in the soil mixture. Where the chemical reacts among the stabilizer and the soil, this process will enhance the sample's durability and mechanical properties. The SCBA was pozzolanic material with a high amount of silica which is suitable for partial blending components for cement. This partial replacement will reduce the problem of waste disposal (SCBA), environmental pollution from the emission of CO_2 (cement), and water pollution.

The result from the study shows that the addition of SCBA enhanced the structure of the blend materials and prominent to a more excellent value of strength. The primary hydration happens after the cement and water react to gain initial strength due to the composition of cementitious products. The process continues with secondary hydration, where the pozzolanic reaction fills pores in the soil system with fine particles from SCBA.

The statement was supported by the result in this study, where when the amount of cement used was the same, and the percentage of SCBA increased, the strength likewise kept on escalating. This condition occurs because of the pozzolanic result and decreasing capillary openings. Thus, from the justification, the amount of cement could be reduced and replaced by partial SCBA to get better results than the cement alone. Besides that, it is worth noticing that the blended Cement-SCBA-Soil sample mixtures achieved compressive strength superior to initial untreated soil, mainly when the 10% cement and 9% of SCBA with seven days curing time are used.

Furthermore, the volume of compressibility of Cement-SCBA-Soil reduced compared to the natural untreated soil. The result indicated that using SCBA as partial cement reinforcement enhances

the stiffness of the soil matrix and can be used to overcome difficulties in construction such as excessive settlement and lead structural damage to the building frame or loss of functionality. Therefore, the blend of SCBA and cement as a partial substitute for cementing the stabilization of problematic soil appears to be a favorable option after pondering economic, energy utilization, pollution, and sustainability concerns.

CONCLUSION

The utilization of waste materials due to industrial and agricultural activities has become a great concern to the developing country. These unwelcome wastes have affected the atmosphere because of the challenge of management and disposal. In this research, the effect of SCBA has been studied on Compressive Strength and Soil Compressibility. The higher the percentages of SCBA used, the better the soil compressive strength. Furthermore, the strength value of the stabilized soil improved as the curing period increased. Additionally, the compressibility of cement-treated soil was reduced with the addition of SCBA. Adding 3% of SCBA to the cement-treated soil seems to be the optimum value, at least at a small loading stage. Using SCBA as a partial substitute for OPC gives positive results in stabilizing the soil. However, no optimum amount of SCBA was found in the study. Therefore, future studies may consider higher content of SCBA, which is larger than the maximum amount used in this study. In conclusion, SCBA could be used as an alternative additive to improve soil behaviour in strength and compressibility with or without cement. Consequently, applying bagasse ash waste in the ground improvement has excellent potential for the future to solve specific waste disposal problems.

REFERENCES

Huat, B. B. K., Maail, S., and Mohamed, T. A. (2005) Effect of Chemical on the Engineering Properties of Tropical Peat Soil. *American Journal of Applied Sciences, Science Publication,* 1113-1120.

Gueddouda, M. K., Goual, I., Lamara, M., Smaida, A., and Mekarta, B. (2011) Chemical Stabilization of Expansive Clays from Algeria. G*lobal Journal of Researches in Engineering: J General Engineering,* **11(5),** Ver 1.

Abu Talib, M. K., Nuriyuki, Y., and Ishikura, R. (2015) Effects of sugarcane bagasse ash (SCBA) on the strength and compressibility of cement stabilized peat. *Lowland Technology International,* **17(2),** 73-82.

Kishor Kumar, V., Vandhana Devi, V., and Rajan, N. K. (2020) Effect of Sugarcane Bagasse Ash and Cement on the Engineering Properties of Soft Clay Soil. *International Journal of Advance Science and Technology,* **29(10),** 6919-6926.

Onyelowe, K. C. (2012) Cement stabilized Akwuete lateritic soil and the use of bagasse ash as Admixture. *Int. J. Sci. Eng. Investig.*, **1(2).**

Adhikary, S. and Jana, K. (2016) Potentials of Rice-Husk Ash as A Soil Stabilizer. *International Journal of Latest Research in Engineering and Technology (IJLRET),* **2(2),** 40-48.

Roy, A. (2014) Soil Stabilization using Rice Husk Ash and Cement. *International Journal of Civil Engineering Research,* **5(1),** 49-54.

Xiao, H., and Lee, F. (2019). Curing time effect on behavior of cement treated marine clay. *Int. J. Eng. Phys. Sci,* **Vol. 43,** 71-78.

Muhunthan, B., and Sariosseiri, F. (2018) Interpretation of geotechnical properties of cement treated soils (No. WA-RD 715.1). Washington (State). Department of Transportation.

Reang, R. and Kumar Pal, S. (2019) Strength behaviours of the clayey-silt soil mixed with fly ash and sand. *Ground Improvement Techniques and Geosynthetics,* 105-113.

Hakari, U. D., and Puranik, S. C. (2012) Stabilisation of Black Cotton Soils Using Fly Ash. Hubballi-Dharwad Municipal Corporation Area, Karnataka, India. *Global Journal of researches in engineering Civil and Structural engineering*, **12(2),** Version 1.0.

Chittaranjan, M., Vijay, M., and Keerthi, D. (2011) Agricultural wastes as soil stabilizers. *International Journal of Earth Sciences and Engineering*, **4(6),** 50-51.

Sarkar, R., Abbas, S. M., and Shahu, J. T. (2012) A comparative study of geotechnical behavior of lime stabilized pond ashes from Delhi region. *International Journal on GEOMATE, Japan*, **3(1),** 273-279

WBCSD, (2019) Cement Technology Roadmap 2009. World Business Council for Sustainable Development, W.B.C.S.D. *France: International Energy Agency, I.E.A.*

Frías, M., Villar-Cociña, E., and Valencia-Morales, E. (2007) Characterisation of sugar cane straw waste as pozzolanic material for construction: Calcining temperature and kinetic parameters. *Waste Management*, **27**, 533-538.

Rajakumar, C., Meenambal, T., and Arumairaj, P. D. (2014) California bearing ratio of expansive subgrade stabilized with waste materials. *International Journal of Advanced Structures and Geotechnical Engineering,* **3**.

Muangtong, P., Sujjavanich, S., Boonsalee, S., Poomiapiradee, S., and Chaysuwan, D. (2013) Effects of fine bagasse ash on the workability and compressive strength of Mortars. *Chiang Mai Journal of Science*, **40(1),** 126-134.

Paula Gisele, L. D. P., Daniel, M., Andrew, H., and Pete, W. (2016) Cement with SCBA as a stabilizer

in compressed earth blocks. *Terra 2016, 12th World Congress on Earthen Architecture.*

Pachori, C., and Saxena, A. (2019) Stabilization of Subgrade Soil Using Sugarcane Bagasse Ash (SCBA). *International Research Journal of Engineering and Technology (IRJET)*, **6(12)**.

Kamaruidzaman, N. S. Abu Talib, M. K. Alias. Nurul Amirah, Z. Adnan, A. Madun, H. Zainal Abidin Aziman, Z., Hazreek, . A., Md, M. F., and Dan, N. A. (2019) Peat Stabilization by Using Sugarcane Bagasse Ash (SCBA) as a Partial Cement Replacement Materials. International Journal of Integrated Engineering, **11(6),** 204-213.

Mikhail, M., Keramatikerman, M., Chegenizadeh, A., Terzaghi, S., Burns, G., and Nikraz, H. (2020) Influence of Bagasse Ash on Compaction Behvaiour of Soil. *International Journal of Innovative Technology and Exploring Engineering (IJITEE),* **9(5)**.

Xu, Q., Ji, T., SJi Gao, Yang, Z., and Wu, N. (2018) Characteristics and Applications of Sugar Cane Bagasse Ash Waste in Cementitious Materials. *Materials*.

Keramatikerman, M., Chegenizadeh, A., and Terzaghi, S. (2019) Review on Effect of Sugarcane Bagasse Ash as an Additive in Construction Industry. *EJGE,* **24**, 453-470.

Abbasi, A and Zargar, A. (2013) Using baggase ash in concrete as pozzolan. *Middle East Journal of Scientific Research,* **13(6),** 716-719.

Kantinaris, N. (2004) Re-cycling of sugar-ash: a raw feed material for rotary kilns. *Waste Management*, **24**, 999-1004.

Saini, H., Khatti, J., and Acharya, B. (2019) Stabilization of Black Cotton Soil by Using Sugarcane Bagasse Ash. *International Journal of Scientific Research and Review,* **7(1)**, 109-116.

Kharade, AS., Suryavanshi, V. V., Gujar, B. S., and Deshmukh, R. R. (2014) Waste product Bagasse Ash from Sugar Industry can be used as Stabilizing material for Expansive Soils. *International Journal of Research in Engineering and Technology*, **3(3),** 506-512.

Abu Talib M. K., and Nuriyuki, Y. (2017) Highly Organic Soil Stabilization by Using Sugarcane Bagasse Ash (SCBA). *MATEC Web of Conferences, **103**:07013*

Chegenizadeh, A., Keramatikerman, M., Miceli, S., Nikraz, H., and Salih Sabbar, A. (2020) Investigation on Recycled Sawdust in Controlling Sulphate Attack in Cemented Clay. *Applied Sciences*

Sharma, T., and Kaushik, R. (2019) Effect of Polypropylene Fiber on Properties of Bagasse Ash-Cement Stabilized Clay Soil. *International Journal on Emerging Technologies,* **10(2),** 255-266.

Nagataki, S. (1994) Mineral admixtures in concrete: state of the art and trends. *Special Publ.*

Joshaghani, A., Ramezanianpour, A. A., and Rostami, H. (2016) Effect of incorporating Sugarcane Bagasse Ash (SCBA) in mortar to examine durability of sulfate attack. *International Conference on Concrete Sustainability.*

Khan, S., Kamal, M., and Haroon, M. (2015) Potential of cement treated sugar cane bagasse ash (SCBA) as highway construction Material. *Road & Transport Research,* **24(3).**

Amu, O. O., Ogunniyi, S. A., and Oladeji, O. O. (2011) Geotechnical properties of lateritic soil stabilized with sugarcane straw ash. *American Journal of Scientific and Industrial Research,* **2(2),** 323-331. Doi:10.5251/ajsir.2011.2.2.323.331

Rahman, M. M. A., Rabbi, T. M. Z., and Siddique, A. (2011) Strength and Deformation Characteristics of Cement Treated Soft Bangladesh Clays. *Journal - The Institution of Engineers, Malaysia*, **72(4).**

Rong-rong, Z. and Dong-dong, M. (2020) Effects of Curing Time on the Mechanical Property and Microstructure Characteristics of Metakaolin-Based Geopolymer Cement-Stabilized Silty Clay. *Advances in Materials Science and Engineering*.

Hossain, K. M. A, & Mol, L. (2011) Some engineering properties of stabilized clayey soils incorporating natural pozzolans and industrial wastes. *Construction and Building Materials,* **25(8),** 3495-3501.